JOURNAL OF AEROSPACE INFORMATION SYSTEMS
Vol. 23, No. 7, July 2026

Software Architecture of Sequentially Rotating Rigid Spacecraft Components Using the Backsubstitution Method

João Vaz Carneiro*
University of Colorado Boulder, Boulder, Colorado 80303
Cody Allard†
Laboratory for Atmospheric and Space Physics, Boulder, Colorado 80303
and
Hanspeter Schaub‡
University of Colorado Boulder, Boulder, Colorado 80303

https://doi.org/10.2514/1.I011695

Spacecraft simulations and subsequent analyses are critical to verifying performance requirements in any mission development. With increasingly more complex spacecraft configurations, finding the fully coupled equations of motion and developing an integrated dynamics and flight software simulation architecture that configures such complex dynamics is difficult and often spacecraft-specific. Rotating appendages are a particularly interesting subcategory because they represent many common components, from spinning attitude control devices and flexible solar panels to robotic arms used to service and dock spacecraft. This work builds on the backsubstitution method (BSM), which introduced a modular and fast-to-execute framework to represent the equations of motion, assuming that the spacecraft comprises multiple effectors attached to a rigid hub. A novel modular software architecture enables the BSM simulation of any sequentially connected rotating appendages and the equations of motion that represent spacecraft with these components (or effectors). The rigid bodies can be connected by any sequence of single-axis rotations with any mass distribution or spin axis, vastly expanding the possible BSM spacecraft configurations and allowing for the simulation of complex effectors attached to a rigid hub under a common framework. Numerical examples of a flexible panel and a robotic arm illustrate the effectiveness of this modeling approach.

Nomenclature

A_c	=	center-of-mass location of body A
$\boldsymbol{a}_{ij}$	=	effector backsubstitution term for $\ddot{\boldsymbol{r}}_{B/N}$
$\dot{\boldsymbol{a}}$, $\ddot{\boldsymbol{a}}$	=	first- and second-order time derivatives of vector $\boldsymbol{a}$ with respect to the inertial frame $\mathcal{N}$
$\boldsymbol{a}'$, $\boldsymbol{a}''$	=	first- and second-order time derivatives of vector $\boldsymbol{a}$ with respect to the body frame $\mathcal{B}$
$[\tilde{\boldsymbol{a}}]$	=	cross-product operator written in matrix form
$\boldsymbol{b}_{ij}$	=	effector backsubstitution term for $\dot{\boldsymbol{\omega}}_{B/N}$
C	=	center-of-mass location of the system
$\boldsymbol{c}$	=	vector from point B to the center of mass of the spacecraft C, m
$\boldsymbol{c}_{ij}$	=	independent effector backsubstitution term
$\boldsymbol{F}_{\text{ext}}$	=	vector sum of external forces on the spacecraft, N
$[I_{\text{A},A}]$	=	inertia tensor of body A with respect to point A, $\text{kg}\cdot\text{m}^2$
$\boldsymbol{L}_B$	=	vector sum of external torques on the spacecraft about point B, $\text{N}\cdot\text{m}$
m_{A}	=	mass of body A, kg
N, B, S	=	origin point for inertial, body, and component frames
$\mathcal{N}$, $\mathcal{B}$, $\mathcal{S}$	=	inertial, body, and component frames
$\boldsymbol{r}_{A/B}$, $\dot{\boldsymbol{r}}_{A/B}$, $\ddot{\boldsymbol{r}}_{A/B}$	=	position (m), inertial velocity (m/s), and inertial acceleration (m/s^2) of point A with respect to B
u_S	=	scalar torque applied to the hinge, $\text{N}\cdot\text{m}$
θ, $\dot{\theta}$, $\ddot{\theta}$	=	hinge's angle (rad), angle rate (rad/s), and angle acceleration (rad/s^2)
$\boldsymbol{\sigma}_{\mathcal{A}/\mathcal{B}}$	=	attitude of frame $\mathcal{A}$ with respect to frame $\mathcal{B}$ expressed in modified Rodrigues parameters
$\boldsymbol{\omega}_{\mathcal{A}/\mathcal{B}}$, $\dot{\boldsymbol{\omega}}_{\mathcal{A}/\mathcal{B}}$	=	angular velocity (rad/s) and inertial acceleration (rad/s^2) of frame $\mathcal{A}$ with respect to $\mathcal{B}$

Subscripts

hub	=	spacecraft's hub
i	=	ith component body
sc	=	spacecraft system

I. Introduction

SPACE vehicle design, along with its associated dynamics and control performance analysis process, has become increasingly complex to support ambitious and often rapidly evolving mission requirements. Figure 1 showcases the evolution of spacecraft design with some example missions. Starting with Sputnik 1 [1], the first artificial satellite composed of a sphere with some sensors and four boom antennas, spacecraft design has changed dramatically as technology has evolved. The International Space Station [2] (ISS) has been in orbit for over two decades and is arguably the most complex space vehicle of the 21st century. Notably, many spacecraft now include multilink robotic arms to perform in-orbit operations like servicing and docking. The Canadarm [3–5] has been used by the Space Shuttle (Canadarm 1) and the ISS (Canadarm 2), with plans for using it on Lunar Gateway (Canadarm 3). Other servicing vehicles also employ robotic arms for life-extension and servicing missions. Northrop Grumman's Mission Extension Vehicle [6] attaches thrusters at the end of robotic arms as a means of thrust vectoring. Astroscale UK's upcoming COSMIC mission [7] uses a robotic arm to remove two inactive British satellites currently orbiting Earth.

Presented as Paper 23-192 at the 2023 AAS Astrodynamics Specialist Conference, Big Sky, MT, August 13–17, 2023; received 18 May 2025; accepted for publication 14 February 2026; published online 30 March 2026.

*Graduate Research Assistant, Ann & H.J. Smead Department of Aerospace Engineering Sciences; joao.carneiro@colorado.edu. Member AIAA.

†Guidance, Navigation and Control Engineer, Laboratory for Atmospheric and Space Physics.

‡Schaden Leadership Chair, Professor, Ann & H.J. Smead Department of Aerospace Engineering Sciences. Fellow AIAA.

a) Sputnik* b) Canadarm 2† c) Mission extension vehicle‡

Fig. 1 Examples of space vehicles.

The need for robotic manipulators in space is clear, and the industry will rely on them for future missions [8] with different applications. To achieve this, the vehicle must be thoroughly simulated and analyzed to ensure that the spacecraft meets orbital and pointing mission requirements. This analysis requires an integrated simulation of high-fidelity dynamics, actuator and sensor models, and flight software integration. These steps require deriving and validating the equations of motion that describe the vehicle's dynamic behavior in orbit. However, simulating multi-axis appendages (also called effectors) is challenging due to their numerous degrees of freedom and the inherent dynamic coupling between all spacecraft components.[§,¶,**]

One common approach is to assume that the effector is prescribed [9]; that is, to suppose that each degree of freedom is precisely imposed by an actuator/motor. The outputs of all the actuators would describe the arm's motion. Effectively, this means that the appendage behaves independently of the rigid hub and is not affected by it; however, the rigid hub is still affected by the component's motion. This one-way coupling, which simplifies the equations of motion, is a fair assumption in many applications, such as when modeling imbalanced reaction wheels [10–12] or for certain actuated components [13,14]. Nevertheless, this remains an approximation, and standard validation metrics, such as energy and angular-momentum conservation, are more difficult to apply to verify the simulation's correctness. Therefore, there is a need to rapidly simulate multi-degree-of-freedom effectors that account for the two-way coupling between the hub and the component.

Even when the fully coupled equations of motion are used, they are often developed for a specific effector type, which means that the equations of motion must be rederived and revalidated each time a different effector is required. However, many components are equivalent from a dynamic standpoint, meaning that the same general set of equations can describe them. This idea was first introduced in Vaz Carneiro et al. (2024), which develops particular effector solutions for one- and two-degree-of-freedom effectors [15]. The equations of motion are derived and implemented in a general manner, avoiding the symmetry assumptions of prior work [16,17], allowing the simulation of any part mounted on a single or dual gimbal. The result is a general formulation for each effector type (single- or dual-axis rotating rigid body) that can simulate reaction wheels (single-axis), solar panels (single- or dual-axis), control-moment gyroscopes (dual-axis), and similar systems, using a single set of equations for each type. The general equations are validated once and can be used for current and future implementations of one- and two-degree-of-freedom components, thereby saving users and developers time.

Another important consideration is the ability to readily change the spacecraft configuration. If the equations are developed only for a particular design, they must be changed whenever the configuration changes, which is time-consuming. Modularity in the equations of motion enables analysis of multiple designs without rederiving the equations or rewriting the modules, thereby facilitating rapid development and the addition of new components. This idea was introduced by the backsubstitution method (BSM) [18–20], which rearranges the equations of motion for each effector and the hub into a standard form. In BSM, effectors are dynamic components added to a central, rigid spacecraft hub (core). In turn, instead of having to invert a large system mass matrix, which is computationally very expensive, BSM first solves for the translational and rotational accelerations of the hub $\ddot{\boldsymbol{r}}_{B/N}$ and $\dot{\boldsymbol{\omega}}_{\mathcal{B}/\mathcal{N}}$, respectively, by having already analytically backsubstituted the effector equations of motion into the hub differential equations. Next, the degrees of freedom of each effector are solved with the hub accelerations [18,19]. An alternative formulation is the Spatial Operator Algebra (SOA) [21–23], which can describe a wide range of flexible multibody configurations. Instead of writing the equations of motion in a particular form to avoid inverting the system's mass matrix at once, it leverages its properties to invert it in $\mathcal{O}(N)$ instead of $\mathcal{O}(N^3)$ using a recursive algorithm. SOA can simulate multiple bodies with various joint types (rotational and translational).

This paper introduces a novel effector, formulated using the BSM, whose general functionality can model the dynamics of a range of prior effectors, including balanced and imbalanced reaction wheels [16], variable-speed control moment gyroscopes [24], and hinged solar arrays [17]. In contrast to these prior approaches, no assumptions are made on the mass and geometric properties of the components when deriving the system's equations of motion. Therefore, the resulting equations are general and can be applied to a variety of components, with implications for the simulation architecture. To illustrate this, Fig. 2 shows problem statement diagrams of two rotating dual-axis components: Fig. 2a of a spacecraft with a variable-speed control moment gyroscope, and Fig. 2b of a spacecraft with a dual-hinged panel.

The prior approach to modeling these effectors began by making assumptions about each component, particularly the spin axis and the body's mass distribution. For the variable-speed control-moment gyroscope modeled in Ref. [24], it is assumed that the gimbal axis is perpendicular to the wheel spin axis. The center of mass of the wheel is parameterized by scalar parameters L, l, and d, each about the $\hat{\boldsymbol{g}}_g$, $\hat{\boldsymbol{g}}_s$, and $\hat{\boldsymbol{w}}_2$ axes, respectively. For the dual-hinged panel modeled in Ref. [17], the spin axes of both panels are parallel and defined along each $\hat{\boldsymbol{s}}_{i,2}$ axis. The center of mass is parameterized by a scalar d and is assumed to be along the $-\hat{\boldsymbol{s}}_{i,1}$ axis. These assumptions simplify the system's kinematics and facilitate the derivation of its equations of motion, as many cross-coupling terms vanish due to the orthogonality between the center-of-mass location and the spin axis.

In both examples, the effectors represent dual-axis rotating rigid bodies. However, because of their initial premises, the resulting equations of motion differ and are valid only under the initial

[§]https://www.nasa.gov/history/dawn-of-the-space-age/.
[¶]https://www.asc-csa.gc.ca/eng/iss/canadarm2/about.asp.
[**]https://www.northropgrumman.com/what-we-do/space/space-logistics-services.

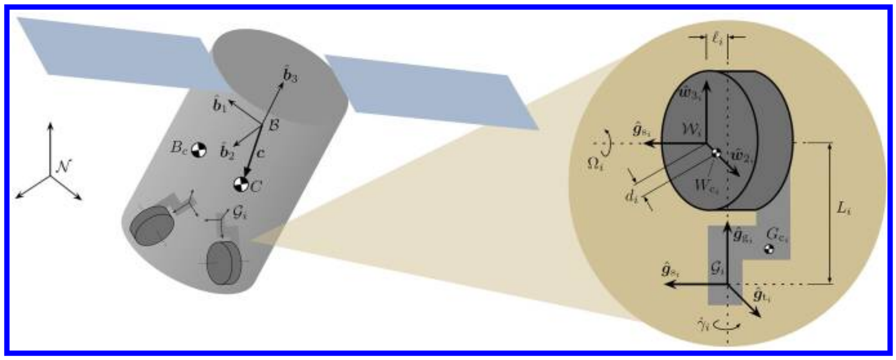

a) Diagram for a variable-speed control moment gyroscope effector [24]

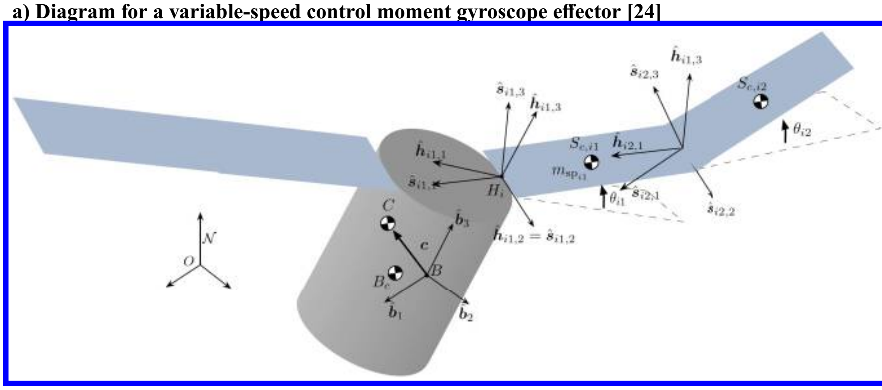

b) Diagram for a dual-hinged solar panel effector [17]

Fig. 2 Diagrams for two different single-axis components.

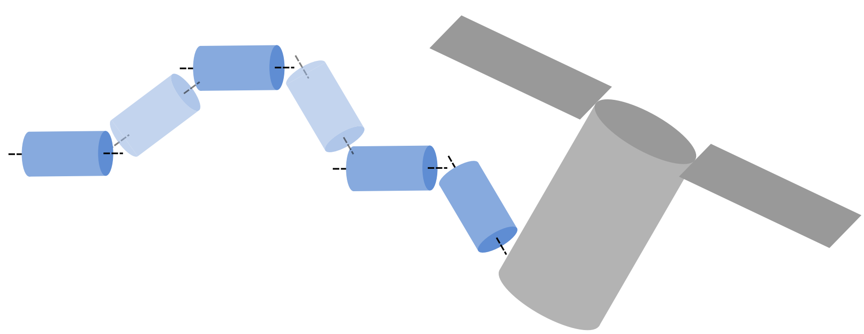

Fig. 3 Simplified problem statement.

assumptions. While this approach accurately describes each effector, it lacks generality; a single standard formulation could have been used with general spin axes and mass distributions to describe both effectors, as they are identical from a dynamic standpoint. Deriving the equations of motion of the system in a general form is a fundamental property of this work.

Many physics simulation software packages are specifically tailored to spacecraft simulations. NASA has developed the open-source 42[††] software to simulate spacecraft with rigid components. Here, the architecture derives the equations of motion for each new subsystem rather than using a centralized formulation. The European Space Agency (ESA) is in charge of SIMULUS-NG,[‡‡] a software package that can replicate complex spacecraft systems, including, for example, batteries, solar panels, thrusters, and the ground station network. It can support analysis of physics simulations and hardware-in-the-loop testing. The Jet Propulsion Laboratory (JPL) has created DARTS/Dshell[§§] [25] software that can simulate a wide range of spacecraft configurations with different actuated components using SOA. While these tools are highly capable, the use of a generalized, centralized implementation of the equations of motion to simulate different components is not addressed. This gap is a central contribution of this paper, specifically to the BSM dynamic modeling framework, as both the software architecture and the general equations are discussed and developed here.

This paper focuses on two novel contributions. First, it develops a general formulation for an effector with N sequentially rotating degrees of freedom connected to a rigid hub, as shown in Fig. 3. It uses the BSM formulation for developing the equations of motion, building on Ref. [15]. Depending on the use case, the dynamicist can determine the number of degrees of freedom required and their arrangement to simulate a particular component, thereby enabling rapid simulation of any sequence of rigid-body components undergoing rotations relative to the spacecraft's hub. Throughout the equations of motion derivation, no assumption is made on the spin axes, the center-of-mass locations, the component inertia, etc. Thus, this paper pursues a universal implementation of these sequentially rotating dynamic subcomponent models. Second, it proposes a software architecture that leverages the generalized equations of motion. It creates a centralized class that contains the mechanics of any rotating component, which can be used to create other effectors.

[††]https://software.nasa.gov/software/GSC-16720-1.
[‡‡]https://esoc.esa.int/content/simulus-ng-new-era-satellite-simulation.
[§§]https://dartslab.jpl.nasa.gov/DSHELL.

The approach is to identify patterns in the effector differential equations of motion, thereby enabling the sequence of rigid bodies to be expressed in summation form. Such a solution retains the ability to describe multiple components that fit the same dynamics type while vastly expanding the configuration space by modeling components with more degrees of freedom. While the rotations considered must be sequential, they can be grouped to form multiple-degree-of-freedom joints. Therefore, the connections between bodies are represented by universal joints, which are one-, two-, or three-dimensional. This technique is particularly useful for robotic arms with joints between links composed of multiple degrees of freedom. This N-degree-of-freedom formulation can also simulate the flexing of rigid bodies, as first proposed in Ref. [17]. It approximates the behavior of a flexible appendage by discretizing it into a series of small rigid bodies connected by joints with springs and dampers. The flexible body modes can be simulated by tuning the spring and damper coefficients. While this is a first-order approximation, it can be useful in early mission design to test for control–structure interactions by ensuring that control devices do not excite unwanted structural modes.

This paper is structured as follows. First, the N-degree-of-freedom effector software architecture is presented. Second, the dynamics formulations used to develop the equations of motion are presented, including Kane's method for deriving the equations and the BSM for writing them in a modular form. The next two sections show the kinematics and the kinetics of the problem. Finally, two scenarios are presented in the numerical example section. The appendix reviews numerical properties used in the development of kinematics and kinetics and discusses the verification procedures for the module.

II. Effector Software Architecture

The software implementation of the spacecraft's equations of motion is an important aspect of any simulation framework. A poorly designed architecture is rigid, does not allow for iterative changes to spacecraft design, has convoluted code that is hard to maintain, and makes future changes difficult for the developer [26,27]. On the contrary, good architecture is modular and dynamic, allowing the engineer to apply any changes that occur during the design phase and to use it for future missions. These properties are especially significant for complex spacecraft simulations in which the vehicle comprises multiple appendages, because the dynamics are fully coupled across all bodies. Therefore, without a well-designed architecture, the code becomes highly intertwined and configuration-specific, making it difficult to add, modify, or remove components and to maintain it.

This section discusses an architecture that unifies the representation of rotating appendages, which are components composed of bodies connected through rotating joints. The joints can have up to three rotational degrees of freedom, as needed, and the number of connected bodies is unlimited. This formulation can represent a wide range of spacecraft components, including reaction wheels, variable-speed control moment gyroscopes, hinged panels, and robotic arms, indicating that the architecture applies to a broad range of spacecraft configurations.

To illustrate the proposed architecture, two examples of a single-axis component are shown. The first is a hinged solar panel [17], shown in Fig. 4a, and the second is an imbalanced reaction wheel [16], shown in Fig. 4b. The panel model assumes that the spin axis is aligned with the hinge frame's $\hat{\boldsymbol{y}}$ axis and that the center of mass is offset along the $-\hat{\boldsymbol{x}}$ axis by a distance d. The hinge frame defines the nominal pose of the panel with respect to the hub's frame. Two types of imbalances parameterize the reaction wheel model. A static imbalance occurs when there is a center-of-mass offset with respect to the spin axis, and a dynamic imbalance happens when the spin axis is not aligned with one of the wheel's principal axes. Besides specifying the location of the hinge point and the associated rotation matrix, the component is defined by the distance d, which corresponds to the center-of-mass offset (if a static imbalance is present), as well as the axial and off-axial inertia terms (if a dynamic imbalance is present).

The particular assumptions of each model yield component-specific equations of motion that must be implemented separately in the code. Figure 5 shows each component's software implementation diagram. Both modules have setup, dynamics, and interface

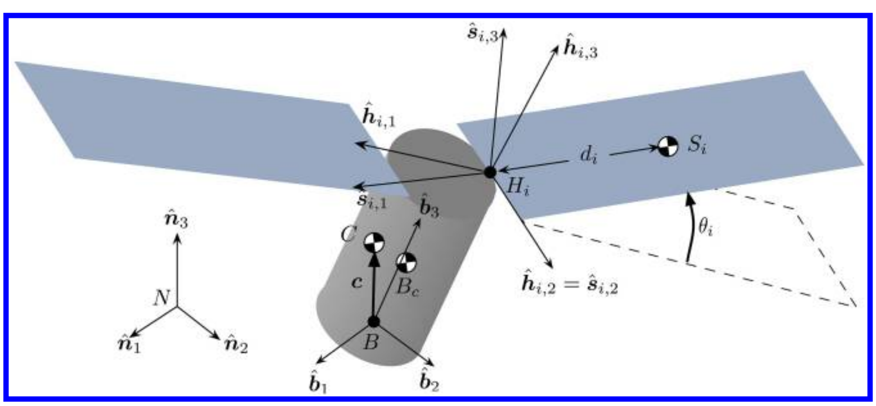

a) Diagram of a single-hinge solar panel [17]

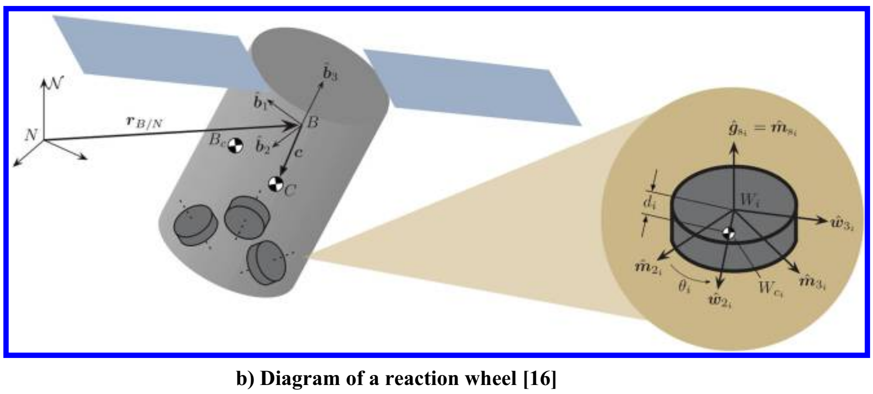

b) Diagram of a reaction wheel [16]

Fig. 4 Diagrams for two different single-axis components.

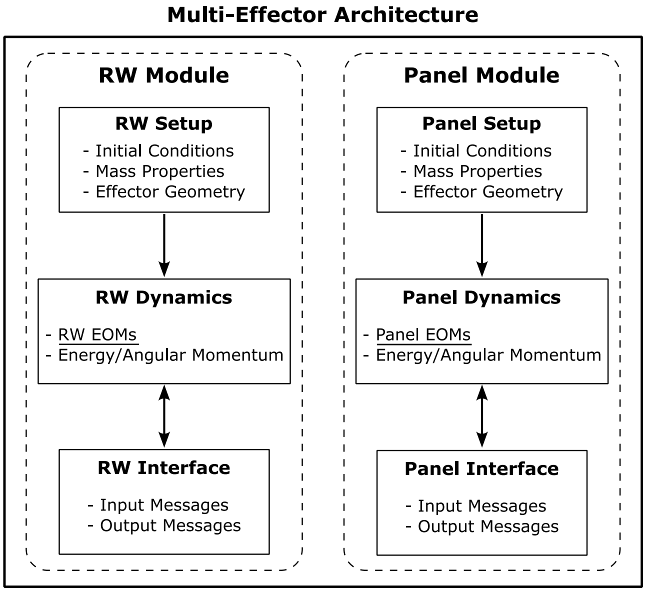

Fig. 5 Software architecture diagram for two different single-axis components using specific dynamics.

sections. The setup layer defines the module's static parameters and its initial conditions. Creating each component individually makes the module setup more intuitive because it is specific to that component. In this example, these include the center-of-mass offset d, the nominal frame pose, the imbalances, and the initial angle and angle rate. The dynamics section defines the kinematics and kinetics of the specific model. Here, the hub-relative positions and velocities are computed from the model's parameters and current states (kinematics), and the component's governing equations of motion are defined (kinetics). This section also computes the component's energy and angular momentum from its kinematics for verification purposes. Finally, the interface layer handles all inputs and outputs. For example, both components can be interfaced with other power modules: the panel's attitude can be used to compute the Sun's incidence angle for power generation, and the reaction wheel's speed can be used to calculate the power draw from the reaction wheel.

The unified module architecture with the general dynamics is shown in Fig. 6. Each module still contains setup, dynamics, and interface layers. However, the dynamics section now uses a general

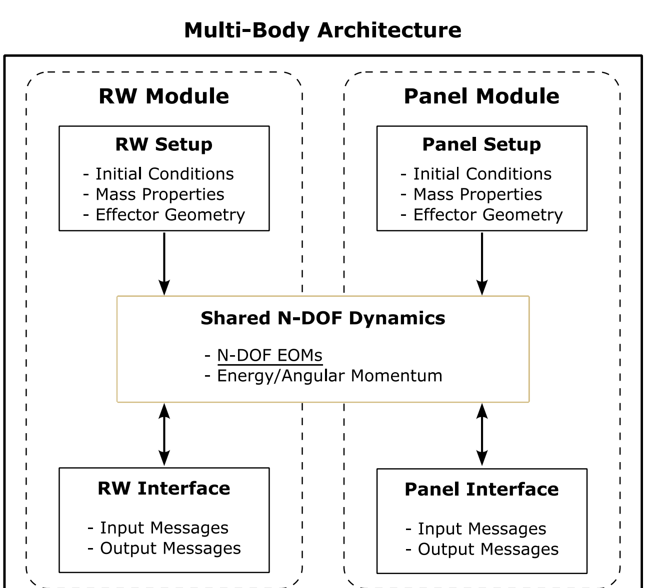

Fig. 6 Software architecture diagram for two different single-axis components using general dynamics.

rather than a component-specific model, thereby decoupling the dynamics of any rotating chained component from its specific properties.

The benefits of this approach are extensive because it decouples the dynamics modeling of a wide range of components into a singular, unified representation in code. First, once the general representation is identified and implemented, the same code can be reused across multiple components, reducing redundancy. This approach makes the code more maintainable since any change to the parent class applies to all downstream modules. Second, it future-proofs the software by enabling the addition of new effectors to the codebase. If a new component meets the criteria for the general dynamics representation, only the setup and interface layers need to be implemented, thereby reducing the time required for mathematical and code development. Finally, the architecture also simplifies module verification and testing. Having a common architecture for this family of components means that centralized, general functions are tested rather than being implemented for a particular component. Therefore, once the common functions are tested (assuming that the test is complex enough to exercise all the different cross-coupling effects), the particular implementations of the general formulation are guaranteed to be correct. A more detailed explanation is given in Appendix B.

The general dynamics layer can be separated into kinematics, kinetics, and testing. The kinematics contains the code that defines the instantaneous pose of each degree of freedom. Multiple degrees of freedom can be defined if the component requires them. To do so, it includes each body's mass and geometric properties, such as the vector from the hinge point to the parent body's hinge point, the location of the center of mass relative to the hinge point, and the inertia about its center of mass. Although it is common to associate a degree of freedom with a physical body, multiple degrees of freedom can be defined in multi-degree-of-freedom joints without mass or inertia. Moreover, kinematics encompasses all hinge properties that connect bodies, such as the rotation axis, spring and damper coefficients, and the initial angle and angle rate. The data contained in the structure must be physical (i.e., the mass cannot be negative), the rotation matrix must be right-handed, etc. The kinetics code implements the system's equations of motion, which can be numerically integrated forward in time to obtain the time history of each degree of freedom. The kinematic information is updated directly from the kinematic model. Finally, the testing element includes the computations that determine the energy and angular-momentum contributions of each degree of freedom, which are used in testing scripts to verify that these quantities are conserved to within machine precision throughout the simulation.

III. Review of Dynamics Formulations

A. Overview of Kane's Method

This paper uses Kane's equations [28,29], as opposed to Newtonian and Eulerian [30,31] formulations employed in prior work [15–18,24,32]. While all formulations are equivalent in that they yield analogous equations of motion, Kane's method is better suited to the N-degree-of-freedom problem. Although more abstract, this work provides deeper analytical insight into the structure of the equations of motion, yielding a general recursive formulation. This property is particularly important because the primary objective is to identify patterns in the equations describing an effector with various degrees of freedom. In addition to Kane's equation, this work uses the inertia transport theorem [33]. Analogous to the vector transport theorem [30], the inertia transport theorem describes the time derivative of the inertia tensor between two different rotating frames. This result simplifies the rotational equations of motion, yielding a more compact analytical solution to the effector's differential equations.

Kane's method, developed by Kane and Levinson, provides analytical insight into the recursive structure of a sequence of rotating bodies. In Ref. [34], the author further adapts this theory to the BSM and introduces the notation used throughout the paper. While this work is agnostic to the dynamics formulation, in the sense that they all yield analogous equations of motion, Kane's method is beneficial for its systematic development of analytical equations of motion. The main challenge in developing the N-degree-of-freedom sequentially spinning effector is identifying patterns in the accelerations that yield compact, programmatic equations of motion, enabling a recursive formula. Kane's method, while more abstract, is structured to facilitate the dynamicist's task of finding all necessary equations of motion. Newtonian or Eulerian formulations require an understanding of internal forces and torques, for example, by drawing the system's bounding box. In contrast, Kane's method requires only the accelerations of the connected bodies. The inertial acceleration vector must be generally expressed as suitable for an unspecified number of degrees of freedom. The resulting equations may need rearrangement before they are ready for use with the backsubstitution formulation, but this can be done using some algebraic properties.

Kane's method begins by defining the generalized coordinates and their corresponding generalized velocities, which need not be the direct derivatives of the coordinates. This property is particularly important in the context of rotational coordinates, where any attitude parameterization can be used, with the angular velocity vector serving as the corresponding generalized velocity.

After defining the generalized coordinate and velocity vectors, the velocity vector of the center of mass and the angular velocity vector of the body's frame are defined. Since rigid bodies are the focus of this work, both translational and rotational properties are investigated. In turn, these vectors are used to determine the partial velocities, which are calculated by taking the derivative of each body's velocity and angular velocity vectors with respect to each generalized velocity coordinate and are defined as

$$\boldsymbol{v}_r^i = \frac{\partial \dot{\boldsymbol{r}}_{S_{c_i}/N}}{\partial u_r} \tag{1}$$

$$\boldsymbol{\omega}_r^i = \frac{\partial \boldsymbol{\omega}_{\mathcal{S}_i/\mathcal{N}}}{\partial u_r} \tag{2}$$

where $\dot{\boldsymbol{r}}_{S_{c_i}/N}$ is the inertial derivative of the center of mass of the ith body, $\boldsymbol{\omega}_{\mathcal{S}_i/\mathcal{N}}$ is the angular velocity of the frame attached to the ith body, and u_r is the rth generalized velocity.

Finally, each degree of freedom defines the generalized active force F_r and the generalized inertia force F_r^*. The active force corresponds to external forces/torques. In contrast, the inertia force is computed using the acceleration of the center of mass of each body and the angular acceleration of each corresponding frame. The generalized active force has a translational and a rotational term applied to forces and torques, respectively, and is defined as

$$F_r = \sum_i (\boldsymbol{v}_r^i)^T \cdot \boldsymbol{F} + \sum_i (\boldsymbol{\omega}_r^i)^T \cdot \boldsymbol{L} \tag{3}$$

where $\boldsymbol{v}_r^i$ and $\boldsymbol{\omega}_r^i$ correspond to the translational and rotational partial velocities of the ith body. Here, the summation is done over all connected bodies. The generalized inertia force also has translational and rotational contributions and is given by

$$\begin{aligned} F_r^* = &-\sum_i (\boldsymbol{v}_r^i)^T \cdot (m_{\mathrm{S}_i} \ddot{\boldsymbol{r}}_{S_{c_i}/N}) \\ &- \sum_i (\boldsymbol{\omega}_r^i)^T \cdot ([I_{\mathrm{S}_i,S_{c_i}}]\dot{\boldsymbol{\omega}}_{\mathcal{S}_i/\mathcal{N}} + [\tilde{\boldsymbol{\omega}}_{\mathcal{S}_i/\mathcal{N}}][I_{\mathrm{S}_i,S_{c_i}}]\boldsymbol{\omega}_{\mathcal{S}_i/\mathcal{N}}) \end{aligned} \tag{4}$$

where $\ddot{\boldsymbol{r}}_{S_{c_i}/N}$ is the acceleration of the center of mass of the ith body, while $\boldsymbol{\omega}_{\mathcal{S}_i/\mathcal{N}}$ and $\dot{\boldsymbol{\omega}}_{\mathcal{S}_i/\mathcal{N}}$ are the angular velocity and angular acceleration of the frame connected to the ith body, respectively. The mass of the ith body is m_{S_i}, and its inertia about its center of mass is $[I_{\mathrm{S}_i,S_{c_i}}]$.

With the generalized active and inertia forces in hand, the equations of motion are defined by

$$F_r + F_r^* = 0 \tag{5}$$

Depending on the variable r, grouping variables in a vector is sometimes convenient instead of using them componentwise. This approach is particularly important for the position $\boldsymbol{r}_{B/N}$ and angular velocity $\boldsymbol{\omega}_{\mathcal{B}/\mathcal{N}}$, where three components are used together to form a vector. In this case, both $\boldsymbol{v}_r$ and $\boldsymbol{\omega}_r$ are matrices instead of vectors, represented by $[\boldsymbol{v}_r^{B_c}]$ and $[\boldsymbol{\omega}_r^{\mathcal{B}}]$, and the forces are vectors instead of scalars: $\boldsymbol{F}_r$ for the generalized active force and $\boldsymbol{F}_r^*$ for the generalized inertia force.

B. Summary of the BSM

While Kane's method is used to derive the equations of motion, the BSM [18] is employed to arrange them into a specific form. Under the assumption that the spacecraft comprises a rigid hub with multiple parallel components, a reasonable assumption for many spacecraft architectures, the BSM writes all equations of motion to avoid inverting the entire system's mass matrix at once. The general structure of the mass matrix under these assumptions is presented in Eq. (6).

$$\begin{bmatrix} [I][\cdot]_{3\times3} & [\cdot]_{3\times3} & [\cdot]_{3\times n_1} & [\cdot]_{3\times n_2} & \cdots & [\cdot]_{3\times n_{N_{\mathrm{st}}}} \\ [\cdot]_{3\times3} & [\cdot]_{3\times3} & [\cdot]_{3\times n_1} & [\cdot]_{3\times n_2} & \cdots & [\cdot]_{3\times n_{N_{\mathrm{st}}}} \\ [\cdot]_{n_1\times3} & [\cdot]_{n_1\times3} & [\cdot]_{n_1\times n_1} & [0]_{n_1\times n_2} & \cdots & [0]_{n_1\times n_{N_{\mathrm{st}}}} \\ [\cdot]_{n_2\times3} & [\cdot]_{n_2\times3} & [0]_{n_2\times n_1} & [\cdot]_{n_2\times n_2} & \cdots & [0]_{n_2\times n_{N_{\mathrm{st}}}} \\ \vdots & \vdots & \vdots & \vdots & \ddots & \vdots \\ [\cdot]_{n_{N_{\mathrm{st}}}\times3} & [\cdot]_{n_{N_{\mathrm{st}}}\times3} & [0]_{n_{N_{\mathrm{st}}}\times n_1} & [0]_{n_{N_{\mathrm{st}}}\times n_2} & \cdots & [\cdot]_{n_{N_{\mathrm{st}}}\times n_{N_{\mathrm{st}}}} \end{bmatrix} \begin{bmatrix} \ddot{\boldsymbol{r}}_{B/N} \\ \dot{\boldsymbol{\omega}}_{\mathcal{B}/\mathcal{N}} \\ \ddot{\boldsymbol{\alpha}}_1 \\ \ddot{\boldsymbol{\alpha}}_2 \\ \vdots \\ \ddot{\boldsymbol{\alpha}}_{N_{\mathrm{st}}} \end{bmatrix} = \begin{bmatrix} [c][\cdot]_{3\times1} \\ [\cdot]_{3\times1} \\ [\cdot]_{n_1\times1} \\ [\cdot]_{n_2\times1} \\ \vdots \\ [\cdot]_{n_{N_{\mathrm{st}}}\times1} \end{bmatrix} \tag{6}$$

The mass matrix has a special structure: the first 6 rows and columns are fully populated, and the main block diagonal is also fully populated. This structure is a consequence of the spacecraft's geometry, with a centralized hub and multiple parallel effectors that do not directly depend on one another. Therefore, only a 6×6 matrix of the hub's translation and rotation states must be inverted, along with any mass matrices for each subcomponent. The resulting set of equations is particularly suitable for software implementation because matrix inversion scales with the cube of the matrix dimension. Moreover, the implementation is fully modular, allowing any number of effectors to be added in parallel without altering the form of the equations.

For the translation equations of motion, the generalized equation is shown here as

$$\begin{aligned} &m_{\mathrm{sc}}\ddot{\boldsymbol{r}}_{B/N} - m_{\mathrm{sc}}[\tilde{\boldsymbol{c}}]\dot{\boldsymbol{\omega}}_{\mathcal{B}/\mathcal{N}} + \sum_{i=1}^{N_{\mathrm{st}}}[\boldsymbol{v}_{\mathrm{Trans,LHS}_i}]\ddot{\boldsymbol{\alpha}}_i \\ &= \sum_{i=1}^{N_{\mathrm{dyn}}}\boldsymbol{F}_i - 2m_{\mathrm{sc}}[\tilde{\boldsymbol{\omega}}_{\mathcal{B}/\mathcal{N}}]\boldsymbol{c}' - m_{\mathrm{sc}}[\tilde{\boldsymbol{\omega}}_{\mathcal{B}/\mathcal{N}}][\tilde{\boldsymbol{\omega}}_{\mathcal{B}/\mathcal{N}}]\boldsymbol{c} + \sum_{i=1}^{N_{\mathrm{st}}}\boldsymbol{v}_{\mathrm{Trans,RHS}_i} \end{aligned} \tag{7}$$

There are a few things to note in the equation above. First, all explicit second-order accelerations are moved to the left-hand side. These include the acceleration of the hub, the angular acceleration of the hub's frame, and all second-order time derivatives of the effector's states. Second, while Eq. (7) sums all effectors, this work derives equations for only one effector, with the results for multiple effectors being analogous. This property is a direct consequence of the modularity of the BSM. Finally, the right-hand side shows some terms using the center-of-mass properties, such as $\boldsymbol{c}$ and $\boldsymbol{c}'$, which correspond to the position and velocity (with respect to the $\mathcal{B}$ frame) of the center of mass with respect to point B, respectively. Therefore, the final equation must be rearranged to make these terms explicit. The remaining terms are grouped into $\boldsymbol{v}_{\text{Trans,RHS}_i}$, which catches any other contributions.

The generalized rotational equation of motion is

$$m_{\text{sc}}[\tilde{\boldsymbol{c}}]\ddot{\boldsymbol{r}}_{B/N} + [I_{\text{sc},B}]\dot{\boldsymbol{\omega}}_{\mathcal{B}/\mathcal{N}} + \sum_{i=1}^{N_{\text{st}}}[\boldsymbol{v}_{\text{Rot,LHS}_i}]\ddot{\boldsymbol{\alpha}}_i$$
$$= \sum_{i=1}^{N_{\text{dyn}}}\boldsymbol{L}_{B_i} - [\tilde{\boldsymbol{\omega}}_{\mathcal{B}/\mathcal{N}}][I_{\text{sc},B}]\boldsymbol{\omega}_{\mathcal{B}/\mathcal{N}} - [I'_{\text{sc},B}]\boldsymbol{\omega}_{\mathcal{B}/\mathcal{N}} + \sum_{i=1}^{N_{\text{st}}}\boldsymbol{v}_{\text{Rot,RHS}_i} \tag{8}$$

As before, the explicit second-order terms are moved to the left-hand side. The right-hand side contains terms using the system mass properties, which now include the system's total inertia $[I_{\text{sc},B}]$ and its $\mathcal{B}$-frame derivative $[I'_{\text{sc},B}]$, as well as the catch-all term $\boldsymbol{v}_{\text{Rot,RHS}_i}$ for all other terms.

Finally, for a single uncoupled degree of freedom, the governing equation of motion for each effector takes the form

$$\ddot{\alpha}_i = \boldsymbol{a}_{\alpha_i}\cdot\ddot{\boldsymbol{r}}_{B/N} + \boldsymbol{b}_{\alpha_i}\cdot\dot{\boldsymbol{\omega}}_{\mathcal{B}/\mathcal{N}} + c_{\alpha_i} \tag{9}$$

where α_i is the state and $\ddot{\alpha}_i$ the corresponding second-order time derivative. The left-hand side is only taken by the states' acceleration, while the right-hand side contains three terms: $\ddot{\boldsymbol{r}}_{B/N}$, $\dot{\boldsymbol{\omega}}_{\mathcal{B}/\mathcal{N}}$, and the last term, which conglomerates all remaining contributions. The equations are written this way because this result for the state acceleration is "backsubstituted" into the translational and rotational equations, which means that $\ddot{\boldsymbol{r}}_{B/N}$ and $\dot{\boldsymbol{\omega}}_{\mathcal{B}/\mathcal{N}}$ can be solved for independently of any $\ddot{\alpha}_i$. The result is then substituted in Eq. (9), and all states can be numerically propagated forward in time because their accelerations have been explicitly solved. However, many effectors have multiple coupled degrees of freedom, meaning the equations do not fit into the form presented in Eq. (9). For these cases, it is useful to write the equations in a coupled form using a mass matrix, as shown below:

$$[\boldsymbol{M}_{\alpha_i}]\ddot{\boldsymbol{\alpha}}_i = [\boldsymbol{A}^*_{\alpha_i}]\ddot{\boldsymbol{r}}_{B/N} + [\boldsymbol{B}^*_{\alpha_i}]\dot{\boldsymbol{\omega}}_{\mathcal{B}/\mathcal{N}} + \boldsymbol{C}^*_{\alpha_i} \tag{10}$$

where $[\boldsymbol{M}_{\alpha}]$ is the mass matrix and $\ddot{\boldsymbol{\alpha}}$ is the stacked vector of states for the effector. In some cases, particularly when the number of degrees of freedom is small, the matrix equation in Eq. (10) can be analytically solved for, yielding several equations like Eq. (9). However, this is not always feasible and can be tedious; a faster option is to invert the mass matrix $[\boldsymbol{M}_{\alpha}]$. As with the global mass matrix, this approach can be computationally expensive, but it is viable because it is applied to each effector rather than to the entire system. Using this approach, the canonical form of Eq. (10) is given by

$$\ddot{\boldsymbol{\alpha}}_i = [\boldsymbol{A}_{\alpha_i}]\ddot{\boldsymbol{r}}_{B/N} + [\boldsymbol{B}_{\alpha_i}]\dot{\boldsymbol{\omega}}_{\mathcal{B}/\mathcal{N}} + \boldsymbol{C}_{\alpha_i} \tag{11}$$

where the new matrices are defined as

$$[\boldsymbol{A}_{\alpha_i}] = [\boldsymbol{M}_{\alpha_i}]^{-1}[\boldsymbol{A}^*_{\alpha_i}], \qquad [\boldsymbol{B}_{\alpha_i}] = [\boldsymbol{M}_{\alpha_i}]^{-1}[\boldsymbol{B}^*_{\alpha_i}],$$
$$\boldsymbol{C}_{\alpha_i} = [\boldsymbol{M}_{\alpha_i}]^{-1}\boldsymbol{C}^*_{\alpha_i} \tag{12}$$

The BSM requires taking Eq. (11) and plugging the result into Eqs. (7) and (8), which removes the explicit dependency of the effector second-order state derivatives from the translational and rotational equations. The result is a 6×6 system of equations in $\ddot{\boldsymbol{r}}_{B/N}$ and $\dot{\boldsymbol{\omega}}_{\mathcal{B}/\mathcal{N}}$ given by

$$\begin{bmatrix} [A] & [B] \\ [C] & [D] \end{bmatrix}\begin{bmatrix} \ddot{\boldsymbol{r}}_{B/N} \\ \dot{\boldsymbol{\omega}}_{\mathcal{B}/\mathcal{N}} \end{bmatrix} = \begin{bmatrix} \boldsymbol{v}_{\text{Trans}} \\ \boldsymbol{v}_{\text{Rot}} \end{bmatrix} \tag{13}$$

Here, $\boldsymbol{v}_{\text{Trans}}$ and $\boldsymbol{v}_{\text{Rot}}$ correspond to all the terms that do not explicitly depend on any second-order time derivatives in the translational and rotational equations of motion, respectively. As discussed in Ref. [18], this system of six equations is solved using the Schur complement matrix formulation for the partitioned form of the hub system mass matrix:

$$\dot{\boldsymbol{\omega}}_{\mathcal{B}/\mathcal{N}} = ([D] - [C][A]^{-1}[B])^{-1}(\boldsymbol{v}_{\text{Rot}} - [C][A]^{-1}\boldsymbol{v}_{\text{Trans}}) \tag{14}$$

$$\ddot{\boldsymbol{r}}_{B/N} = [A]^{-1}(\boldsymbol{v}_{\text{Trans}} - [B]\dot{\boldsymbol{\omega}}_{\mathcal{B}/\mathcal{N}}) \tag{15}$$

Once the accelerations are solved, they can be "backsubstituted" into the effector equation in Eq. (10) to solve for the acceleration of each effector's states. Accordingly, all accelerations are explicitly computed and can be propagated using any numerical integration method.

IV. Kinematics of the N-Degree-of-Freedom Effector

A. Effector Problem Statement

The problem statement for the N-axes (or N-degree-of-freedom since there is one degree of freedom per axis) rotating rigid body effector attached to the hub is given in Fig. 7. The inertial frame $\mathcal{N}$ originates at point N. The spacecraft comprises a rigid hub to which the effector is attached. The $\mathcal{B}$ frame has an origin point at B, which does not have to coincide with the center of mass of the hub B_c nor

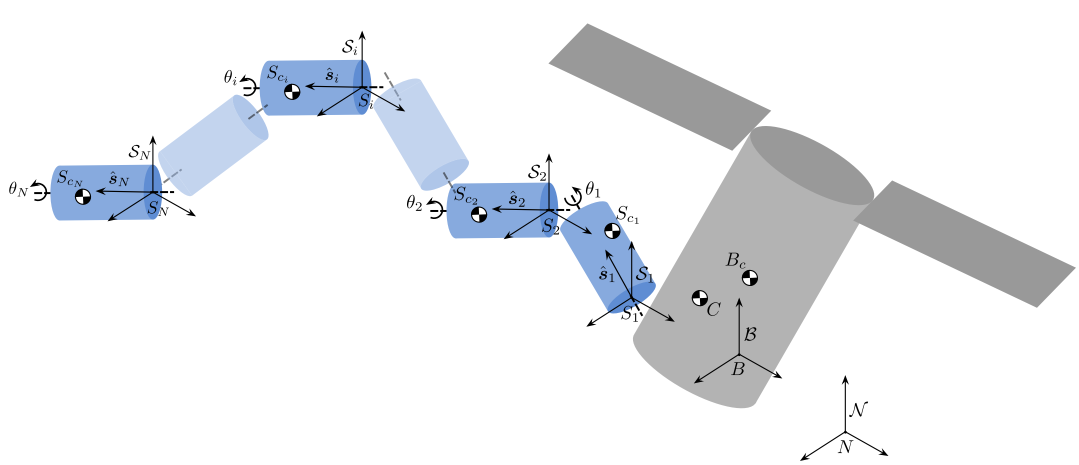

Fig. 7 Problem statement for the N-degree-of-freedom spinning rigid body.

the center of mass of the system C. The hub has mass m_{hub}, center of mass $\boldsymbol{r}_{B_c/B}$, and inertia about its center of mass, $[I_{\text{hub},B_c}]$. The effector consists of a chain of rigid bodies connected through single hinges. The mass and inertia of some bodies can be set to zero to give the joint multiple degrees of freedom of an effector component. Here, the degrees of rotation constitute an Euler angle sequence. Each body has a frame $\mathcal{S}_i$ with origin S_i, mass m_{S_i}, center of mass $\boldsymbol{r}_{S_{c_i}/S_i}$, and inertia about its center of mass $[I_{\mathrm{S}_i,S_{c_i}}]$. The bodies rotate about the $\hat{\boldsymbol{s}}_i$ spin axis, which passes through the origin of the $\mathcal{S}_i$ frame, with an angle θ_i and angular rate $\dot{\theta}_i$.

Kane's method requires defining generalized coordinate and velocity vectors containing the system's states and their derivatives. For this problem, the states include the position and attitude of the hub $\boldsymbol{r}_{B/N}$ and $\boldsymbol{\sigma}_{\mathcal{B}/\mathcal{N}}$, respectively, as well as the angles for all joints of the effector. The generalized coordinate vector $\boldsymbol{q}$ and corresponding generalized velocity vector $\boldsymbol{u}$ are

$$\boldsymbol{q} = \begin{bmatrix} \boldsymbol{r}_{B/N} \\ \boldsymbol{\sigma}_{\mathcal{B}/\mathcal{N}} \\ \theta_1 \\ \theta_2 \\ \vdots \\ \theta_N \end{bmatrix}, \qquad \boldsymbol{u} = \begin{bmatrix} \dot{\boldsymbol{r}}_{B/N} \\ \boldsymbol{\omega}_{\mathcal{B}/\mathcal{N}} \\ \dot{\theta}_1 \\ \dot{\theta}_2 \\ \vdots \\ \dot{\theta}_N \end{bmatrix} \tag{16}$$

Therefore, this problem has $N+6$ state variables: 3 for the translational motion, 3 for the rotational motion, and N for each additional rotation angle. Each state variable requires its equation of motion to be numerically integrated, yielding a time history for each state. These considerations are summarized in Table 1.

B. Translational Kinematics

This subsection aims to find a formula for the position, velocity, and acceleration of the center of mass of the ith body S_{c_i} with respect to the origin of the inertial frame N. It is important to write the formulas in a way that explicitly exposes the system's second-order state derivatives, namely $\ddot{\boldsymbol{r}}_{B/N}$, $\dot{\boldsymbol{\omega}}_{\mathcal{B}/\mathcal{N}}$, and $\ddot{\theta}_i$. The position is

$$\boldsymbol{r}_{S_{c_i}/N} = \boldsymbol{r}_{B/N} + \boldsymbol{r}_{S_{c_i}/S_i} + \sum_{j=1}^{i} \boldsymbol{r}_{S_j/S_{j-1}} \tag{17}$$

The velocity is found by taking the inertial time derivative of the position formula in Eq. (17):

$$\begin{aligned}\dot{\boldsymbol{r}}_{S_{c_i}/N} &= \dot{\boldsymbol{r}}_{B/N} + [\tilde{\boldsymbol{\omega}}_{S_i/N}]\boldsymbol{r}_{S_{c_i}/S_i} + \sum_{j=1}^{i}[\tilde{\boldsymbol{\omega}}_{S_{j-1}/N}]\boldsymbol{r}_{S_j/S_{j-1}} \\ &= \dot{\boldsymbol{r}}_{B/N} - [\tilde{\boldsymbol{r}}_{S_{c_i}/B}]\boldsymbol{\omega}_{\mathcal{B}/\mathcal{N}} - [\tilde{\boldsymbol{r}}_{S_{c_i}/S_i}]\boldsymbol{\omega}_{\mathcal{S}_i/\mathcal{B}} - \sum_{j=1}^{i}[\tilde{\boldsymbol{r}}_{S_j/S_{j-1}}]\boldsymbol{\omega}_{S_{j-1}/B}\end{aligned} \tag{18}$$

It is important to note that the transport theorem is used extensively to simplify some derivatives, particularly by using the property that $\boldsymbol{r}_{S_{c_i}/S_i}$ is constant in the $\mathcal{S}_i$ frame and that $\boldsymbol{r}_{S_i/S_{i-1}}$ is constant in the $\mathcal{S}_{i-1}$ frame. To simplify the expression above, the summation term is further developed:

Table 1 State variables for the N-axis rotating rigid-body spacecraft

State variables	Degrees of freedom	Equations of motion
$\boldsymbol{r}_{B/N}, \dot{\boldsymbol{r}}_{B/N}$	3	Translational
$\boldsymbol{\sigma}_{\mathcal{B}/\mathcal{N}}, \boldsymbol{\omega}_{\mathcal{B}/\mathcal{N}}$	3	Rotational
$\boldsymbol{\theta}, \dot{\boldsymbol{\theta}}$	N	Spinner rotational

$$\begin{aligned}\sum_{j=1}^{i}[\tilde{\boldsymbol{r}}_{S_j/S_{j-1}}]\boldsymbol{\omega}_{S_{j-1}/B} &= \sum_{j=2}^{i}[\tilde{\boldsymbol{r}}_{S_j/S_{j-1}}]\boldsymbol{\omega}_{S_{j-1}/B} \\ &= \sum_{j=1}^{i-1}[\tilde{\boldsymbol{r}}_{S_{j+1}/S_j}]\boldsymbol{\omega}_{S_j/B} \\ &= \sum_{j=1}^{i-1}[\tilde{\boldsymbol{r}}_{S_{j+1}/S_j}]\sum_{k=1}^{j}\hat{\boldsymbol{s}}_k\dot{\theta}_k \\ &= \sum_{j=1}^{i-1}\left(\sum_{k=j}^{i-1}[\tilde{\boldsymbol{r}}_{S_{k+1}/S_k}]\right)\hat{\boldsymbol{s}}_j\dot{\theta}_j \\ &= \sum_{j=1}^{i-1}[\tilde{\boldsymbol{r}}_{S_i/S_j}]\hat{\boldsymbol{s}}_j\dot{\theta}_j\end{aligned} \tag{19}$$

where the following property of double summations is used:

$$\sum_{i=1}^{N}\sum_{j=1}^{i} f_{ij} = \sum_{i=1}^{N}\sum_{j=i}^{N} f_{ji} \tag{20}$$

The proof of this property can be found in Appendix A. Substituting the above result into Eq. (18) yields

$$\begin{aligned}\dot{\boldsymbol{r}}_{S_{c_i}/N} &= \dot{\boldsymbol{r}}_{B/N} - [\tilde{\boldsymbol{r}}_{S_{c_i}/B}]\boldsymbol{\omega}_{\mathcal{B}/\mathcal{N}} - [\tilde{\boldsymbol{r}}_{S_{c_i}/S_i}]\boldsymbol{\omega}_{\mathcal{S}_i/\mathcal{B}} - \sum_{j=1}^{i}[\tilde{\boldsymbol{r}}_{S_j/S_{j-1}}]\boldsymbol{\omega}_{S_{j-1}/B} \\ &= \dot{\boldsymbol{r}}_{B/N} - [\tilde{\boldsymbol{r}}_{S_{c_i}/B}]\boldsymbol{\omega}_{\mathcal{B}/\mathcal{N}} - [\tilde{\boldsymbol{r}}_{S_{c_i}/S_i}]\sum_{j=1}^{i}\hat{\boldsymbol{s}}_j\dot{\theta}_j - \sum_{j=1}^{i-1}[\tilde{\boldsymbol{r}}_{S_i/S_j}]\hat{\boldsymbol{s}}_j\dot{\theta}_j\end{aligned} \tag{21}$$

Therefore, the pattern for the velocity of the center of mass of the ith rotating body is

$$\dot{\boldsymbol{r}}_{S_{c_i}/N} = \dot{\boldsymbol{r}}_{B/N} - [\tilde{\boldsymbol{r}}_{S_{c_i}/B}]\boldsymbol{\omega}_{\mathcal{B}/\mathcal{N}} - \sum_{j=1}^{i}[\tilde{\boldsymbol{r}}_{S_{c_i}/S_j}]\hat{\boldsymbol{s}}_j\dot{\theta}_j \tag{22}$$

The acceleration of the center of mass is found by taking an inertial derivative of the velocity found in Eq. (22)

$$\begin{aligned}\ddot{\boldsymbol{r}}_{S_{c_i}/N} &= \ddot{\boldsymbol{r}}_{B/N} - [\tilde{\boldsymbol{r}}_{S_{c_i}/B}]\dot{\boldsymbol{\omega}}_{\mathcal{B}/\mathcal{N}} + [\tilde{\boldsymbol{\omega}}_{\mathcal{B}/\mathcal{N}}]\dot{\boldsymbol{r}}_{S_{c_i}/B} - \sum_{j=1}^{i}[\tilde{\boldsymbol{r}}_{S_{c_i}/S_j}]\hat{\boldsymbol{s}}_j\ddot{\theta}_j \\ &\quad - \sum_{j=1}^{i}[\tilde{\boldsymbol{r}}_{S_{c_i}/S_j}][\tilde{\boldsymbol{\omega}}_{\mathcal{S}_{j-1}/\mathcal{N}}]\hat{\boldsymbol{s}}_j\dot{\theta}_j + \sum_{j=1}^{i}[\tilde{\boldsymbol{\omega}}_{S_j/S_{j-1}}]\dot{\boldsymbol{r}}_{S_{c_i}/S_j}\end{aligned} \tag{23}$$

The transport theorem $\dot{(\cdot)} = (\cdot)' + [\tilde{\boldsymbol{\omega}}_{\mathcal{B}/\mathcal{N}}](\cdot)$ is used to simplify the equation above [30], along with $\boldsymbol{\omega}_{\mathcal{S}_j/\mathcal{N}} = \boldsymbol{\omega}_{\mathcal{S}_j/\mathcal{B}} + \boldsymbol{\omega}_{\mathcal{B}/\mathcal{N}}$ to get

$$\begin{aligned}\ddot{\boldsymbol{r}}_{S_{c_i}/N} &= \ddot{\boldsymbol{r}}_{B/N} - [\tilde{\boldsymbol{r}}_{S_{c_i}/B}]\dot{\boldsymbol{\omega}}_{\mathcal{B}/\mathcal{N}} + [\tilde{\boldsymbol{\omega}}_{\mathcal{B}/\mathcal{N}}][\tilde{\boldsymbol{\omega}}_{\mathcal{B}/\mathcal{N}}]\boldsymbol{r}_{S_{c_i}/B} + [\tilde{\boldsymbol{\omega}}_{\mathcal{B}/\mathcal{N}}]\boldsymbol{r}'_{S_{c_i}/B} \\ &\quad - \sum_{j=1}^{i}[\tilde{\boldsymbol{r}}_{S_{c_i}/S_j}]\hat{\boldsymbol{s}}_j\ddot{\theta}_j - \sum_{j=1}^{i}[\tilde{\boldsymbol{r}}_{S_{c_i}/S_j}][\tilde{\boldsymbol{\omega}}_{\mathcal{S}_{j-1}/\mathcal{B}}]\hat{\boldsymbol{s}}_j\dot{\theta}_j \\ &\quad - \sum_{j=1}^{i}[\tilde{\boldsymbol{r}}_{S_{c_i}/S_j}][\tilde{\boldsymbol{\omega}}_{\mathcal{B}/\mathcal{N}}]\hat{\boldsymbol{s}}_j\dot{\theta}_j + \sum_{j=1}^{i}[\tilde{\boldsymbol{\omega}}_{\mathcal{S}_j/\mathcal{S}_{j-1}}][\tilde{\boldsymbol{\omega}}_{\mathcal{B}/\mathcal{N}}]\boldsymbol{r}_{S_{c_i}/S_j} \\ &\quad + \sum_{j=1}^{i}[\tilde{\boldsymbol{\omega}}_{\mathcal{S}_j/\mathcal{S}_{j-1}}]\boldsymbol{r}'_{S_{c_i}/S_j}\end{aligned} \tag{24}$$

To simplify the above expression, note that

$$\sum_{j=1}^{i}[\tilde{\boldsymbol{\omega}}_{\mathcal{S}_j/\mathcal{S}_{j-1}}][\tilde{\boldsymbol{\omega}}_{\mathcal{B}/\mathcal{N}}]\boldsymbol{r}_{S_{c_i}/S_j} - \sum_{j=1}^{i}[\tilde{\boldsymbol{r}}_{S_{c_i}/S_j}][\tilde{\boldsymbol{\omega}}_{\mathcal{B}/\mathcal{N}}]\hat{\boldsymbol{s}}_j\dot{\theta}_j$$
$$= [\tilde{\boldsymbol{\omega}}_{\mathcal{B}/\mathcal{N}}]\sum_{j=1}^{i}[\tilde{\boldsymbol{\omega}}_{\mathcal{S}_j/\mathcal{S}_{j-1}}]\boldsymbol{r}_{S_{c_i}/S_j} = [\tilde{\boldsymbol{\omega}}_{\mathcal{B}/\mathcal{N}}]\boldsymbol{r}'_{S_{c_i}/B} \tag{25}$$

The final inertial translational acceleration for the ith body is

$$\ddot{\boldsymbol{r}}_{S_{c_i}/N} = \ddot{\boldsymbol{r}}_{B/N} - [\tilde{\boldsymbol{r}}_{S_{c_i}/B}]\dot{\boldsymbol{\omega}}_{\mathcal{B}/\mathcal{N}} - \sum_{j=1}^{i}[\tilde{\boldsymbol{r}}_{S_{c_i}/S_j}]\hat{\boldsymbol{s}}_j\ddot{\theta}_j$$
$$+ [\tilde{\boldsymbol{\omega}}_{\mathcal{B}/\mathcal{N}}][\tilde{\boldsymbol{\omega}}_{\mathcal{B}/\mathcal{N}}]\boldsymbol{r}_{S_{c_i}/B} + 2[\tilde{\boldsymbol{\omega}}_{\mathcal{B}/\mathcal{N}}]\boldsymbol{r}'_{S_{c_i}/B}$$
$$+ \sum_{j=1}^{i}[\tilde{\boldsymbol{\omega}}_{\mathcal{S}_j/\mathcal{S}_{j-1}}]\boldsymbol{r}'_{S_{c_i}/S_j} - \sum_{j=1}^{i-1}[\tilde{\boldsymbol{r}}_{S_{c_i}/S_{j+1}}][\tilde{\boldsymbol{\omega}}_{\mathcal{S}_j/\mathcal{B}}]\boldsymbol{\omega}_{\mathcal{S}_{j+1}/\mathcal{S}_j} \tag{26}$$

C. Rotational Kinematics

This subsection aims to find the rotational properties of the frame attached to the ith body. The angular velocity of the ith frame is

$$\boldsymbol{\omega}_{\mathcal{S}_i/\mathcal{N}} = \boldsymbol{\omega}_{\mathcal{B}/\mathcal{N}} + \sum_{j=1}^{i}\hat{\boldsymbol{s}}_j\dot{\theta}_j \tag{27}$$

The angular acceleration is found by taking the inertial derivative of the expression above:

$$\dot{\boldsymbol{\omega}}_{\mathcal{S}_i/\mathcal{N}} = \dot{\boldsymbol{\omega}}_{\mathcal{B}/\mathcal{N}} + \sum_{j=1}^{i}\hat{\boldsymbol{s}}_j\ddot{\theta}_j + \sum_{j=1}^{i}[\tilde{\boldsymbol{\omega}}_{\mathcal{S}_{j-1}/\mathcal{N}}]\hat{\boldsymbol{s}}_j\dot{\theta}_j \tag{28}$$

The last term can be simplified:

$$\sum_{j=1}^{i}[\tilde{\boldsymbol{\omega}}_{\mathcal{S}_{j-1}/\mathcal{N}}]\hat{\boldsymbol{s}}_j\dot{\theta}_j = \sum_{j=1}^{i}[\tilde{\boldsymbol{\omega}}_{\mathcal{B}/\mathcal{N}}]\hat{\boldsymbol{s}}_j\dot{\theta}_j + \sum_{j=1}^{i}[\tilde{\boldsymbol{\omega}}_{\mathcal{S}_{j-1}/\mathcal{B}}]\hat{\boldsymbol{s}}_j\dot{\theta}_j$$
$$= -[\tilde{\boldsymbol{\omega}}_{\mathcal{S}_i/\mathcal{B}}]\boldsymbol{\omega}_{\mathcal{B}/\mathcal{N}} - \sum_{j=1}^{i}[\tilde{\boldsymbol{\omega}}_{\mathcal{S}_i/\mathcal{S}_j}]\boldsymbol{\omega}_{\mathcal{S}_j/\mathcal{S}_{j-1}} \tag{29}$$

These results are obtained by applying the transport theorem, which makes use of the fact that $\hat{\boldsymbol{s}}_i$ is constant in both the $\mathcal{S}_i$ and $\mathcal{S}_{i-1}$ frames. Therefore, the pattern for the angular acceleration of the ith rotating body is

$$\dot{\boldsymbol{\omega}}_{\mathcal{S}_i/\mathcal{N}} = \dot{\boldsymbol{\omega}}_{\mathcal{B}/\mathcal{N}} + \sum_{j=1}^{i}\hat{\boldsymbol{s}}_j\ddot{\theta}_j - [\tilde{\boldsymbol{\omega}}_{\mathcal{S}_i/\mathcal{B}}]\boldsymbol{\omega}_{\mathcal{B}/\mathcal{N}} - \sum_{j=1}^{i}[\tilde{\boldsymbol{\omega}}_{\mathcal{S}_i/\mathcal{S}_j}]\boldsymbol{\omega}_{\mathcal{S}_j/\mathcal{S}_{j-1}} \tag{30}$$

D. Partial Velocities Table

The partial velocities are computed by taking the partial derivative of each body's center-of-mass velocity $\dot{\boldsymbol{r}}_{S_{c_i}/N}$ or the frame's angular velocity $\boldsymbol{\omega}_{\mathcal{S}_i/\mathcal{N}}$ with respect to each generalized coordinate rate u_r. Therefore, each entry applies $\partial/\partial u_r$ to the related variable, where 1–3 corresponds to $\dot{\boldsymbol{r}}_{B/N}$, 4–6 to $\boldsymbol{\omega}_{\mathcal{B}/\mathcal{N}}$, and the rest to all $\dot{\theta}_i$.

The partial velocity table is shown in Table 2. Each body has a column corresponding to its velocity $\boldsymbol{v}$ and another for the angular velocity $\boldsymbol{\omega}$. The subscript r denotes a partial with respect to the rth generalized rate, and the superscript denotes which point the quantity is associated with. Therefore, $\boldsymbol{v}_r^{S_{c_i}}$ is the partial of the velocity of the ith body taken at its center of mass with respect to rate r, and $\boldsymbol{\omega}_r^{\mathcal{S}_i}$ is the partial of the angular velocity of the ith body taken at its frame's origin point with respect to rate r.

V. Kinetics of the N-Degree-of-Freedom Effector

A. Translational Equation of Motion

Here, the translational equation of motion for the system consisting of a hub with an N-degree-of-freedom effector is derived. The goal is to write the equation to fit the form proposed in Ref. [18]. The following derivation of the equations of motion accounts for the form of Eq. (7) and writes the equations in the most compact form suitable for use with the BSM.

The generalized active force for the system's translation is given by

$$\boldsymbol{F}_{1\text{–}3} = \boldsymbol{F}_{\text{ext}} \tag{31}$$

where $\boldsymbol{F}_{\text{ext}}$ is the sum of the external forces on the system. The generalized inertia forces are given by

$$\boldsymbol{F}^*_{1\text{–}3} = -\sum_{i=0}^{N} m_{\text{S}_i}[\boldsymbol{v}_{1\text{–}3}^{S_{c_i}}]^T \cdot \ddot{\boldsymbol{r}}_{S_{c_i}/N} \tag{32}$$

where, for ease of notation, $S_0 \equiv B$ and $S_{c_0} \equiv B_c$, making the hub the 0th body. No $\boldsymbol{\omega}_r$ terms appear because their respective partial velocities are equal to zero. Using Kane's method, the translational equation of motion is given by setting $\boldsymbol{F}_{1\text{–}3} + \boldsymbol{F}^*_{1\text{–}3} = \boldsymbol{0}$, which yields

$$\sum_{i=0}^{N} m_{\text{S}_i}\ddot{\boldsymbol{r}}_{B/N} - \sum_{i=0}^{N} m_{\text{S}_i}[\tilde{\boldsymbol{r}}_{S_{c_i}/B}]\dot{\boldsymbol{\omega}}_{\mathcal{B}/\mathcal{N}} - \sum_{i=1}^{N} m_{S_i}\sum_{j=1}^{i}[\tilde{\boldsymbol{r}}_{S_{c_i}/S_j}]\hat{\boldsymbol{s}}_j\ddot{\theta}_j$$
$$= \boldsymbol{F}_{\text{ext}} - 2[\tilde{\boldsymbol{\omega}}_{\mathcal{B}/\mathcal{N}}]\sum_{i=1}^{N} m_{\text{S}_i}\boldsymbol{r}'_{S_{c_i}/B} - [\tilde{\boldsymbol{\omega}}_{\mathcal{B}/\mathcal{N}}][\tilde{\boldsymbol{\omega}}_{\mathcal{B}/\mathcal{N}}]\sum_{i=0}^{N} m_{S_i}\boldsymbol{r}_{S_{c_i}/B}$$
$$- \sum_{i=1}^{N} m_{\text{S}_i}\left(\sum_{j=1}^{i}[\tilde{\boldsymbol{\omega}}_{\mathcal{S}_j/\mathcal{S}_{j-1}}]\boldsymbol{r}'_{S_{c_i}/S_j} - \sum_{j=1}^{i-1}[\tilde{\boldsymbol{r}}_{S_{c_i}/S_{j+1}}][\tilde{\boldsymbol{\omega}}_{\mathcal{S}_j/\mathcal{B}}]\boldsymbol{\omega}_{\mathcal{S}_{j+1}/\mathcal{S}_j}\right) \tag{33}$$

Note here that the explicit second-order acceleration terms are grouped on the left-hand side in the equation above, and many terms are already written in a suitable form according to Ref. [18], particularly ones that allow the use of the system's center-of-mass properties. It is useful to define the following mass property terms:

Table 2 Partial velocities

r	$\boldsymbol{v}_r^{B_c}$	$\boldsymbol{\omega}_r^{\mathcal{B}}$	$\boldsymbol{v}_r^{S_{c_1}}$	$\boldsymbol{\omega}_r^{\mathcal{S}_1}$	$\boldsymbol{v}_r^{S_{c_2}}$	$\boldsymbol{\omega}_r^{\mathcal{S}_2}$	$\dots$	$\boldsymbol{v}_r^{S_{c_i}}$	$\boldsymbol{\omega}_r^{\mathcal{S}_i}$	$\dots$	$\boldsymbol{v}_r^{S_{c_N}}$	$\boldsymbol{\omega}_r^{\mathcal{S}_N}$
$1-3$	$[I_{3\times3}]$	$[0_{3\times3}]$	$[I_{3\times3}]$	$[0_{3\times3}]$	$[I_{3\times3}]$	$[0_{3\times3}]$	$\dots$	$[I_{3\times3}]$	$[0_{3\times3}]$	$\dots$	$[I_{3\times3}]$	$[0_{3\times3}]$
$4-6$	$-[\tilde{\boldsymbol{r}}_{B_c/B}]$	$[I_{3\times3}]$	$-[\tilde{\boldsymbol{r}}_{S_{c_1}/B}]$	$[I_{3\times3}]$	$-[\tilde{\boldsymbol{r}}_{S_{c_2}/B}]$	$[I_{3\times3}]$	$\dots$	$-[\tilde{\boldsymbol{r}}_{S_{c_i}/B}]$	$[I_{3\times3}]$	$\dots$	$-[\tilde{\boldsymbol{r}}_{S_{c_N}/B}]$	$[I_{3\times3}]$
7	$[0_{3\times1}]$	$[0_{3\times1}]$	$[\tilde{\boldsymbol{r}}_{S_{c_1}/S_1}]\hat{\boldsymbol{s}}_1$	$\hat{\boldsymbol{s}}_1$	$[\tilde{\boldsymbol{r}}_{S_{c_2}/S_1}]\hat{\boldsymbol{s}}_1$	$\hat{\boldsymbol{s}}_1$	$\dots$	$[\tilde{\boldsymbol{r}}_{S_{c_i}/S_1}]\hat{\boldsymbol{s}}_1$	$\hat{\boldsymbol{s}}_1$	$\dots$	$[\tilde{\boldsymbol{r}}_{S_{c_N}/S_1}]\hat{\boldsymbol{s}}_1$	$\hat{\boldsymbol{s}}_1$
8	$[0_{3\times1}]$	$[0_{3\times1}]$	$[0_{3\times1}]$	$[0_{3\times1}]$	$[\tilde{\boldsymbol{r}}_{S_{c_2}/S_2}]\hat{\boldsymbol{s}}_2$	$\hat{\boldsymbol{s}}_2$	$\dots$	$[\tilde{\boldsymbol{r}}_{S_{c_i}/S_2}]\hat{\boldsymbol{s}}_2$	$\hat{\boldsymbol{s}}_2$	$\dots$	$[\tilde{\boldsymbol{r}}_{S_{c_N}/S_2}]\hat{\boldsymbol{s}}_2$	$\hat{\boldsymbol{s}}_2$
$\vdots$	$\vdots$	$\vdots$	$\vdots$	$\vdots$	$\vdots$	$\vdots$	$\ddots$	$\vdots$	$\vdots$	$\ddots$	$\vdots$	$\vdots$
$6+i$	$[0_{3\times1}]$	$[0_{3\times1}]$	$[0_{3\times1}]$	$[0_{3\times1}]$	$[0_{3\times1}]$	$[0_{3\times1}]$	$\dots$	$[\tilde{\boldsymbol{r}}_{S_{c_i}/S_i}]\hat{\boldsymbol{s}}_i$	$\hat{\boldsymbol{s}}_i$	$\dots$	$[\tilde{\boldsymbol{r}}_{S_{c_N}/S_i}]\hat{\boldsymbol{s}}_i$	$\hat{\boldsymbol{s}}_i$
$\vdots$	$\vdots$	$\vdots$	$\vdots$	$\vdots$	$\vdots$	$\vdots$	$\ddots$	$\vdots$	$\vdots$	$\ddots$	$\vdots$	$\vdots$
$6+N$	$[0_{3\times1}]$	$[0_{3\times1}]$	$[0_{3\times1}]$	$[0_{3\times1}]$	$[0_{3\times1}]$	$[0_{3\times1}]$	$\dots$	$[0_{3\times1}]$	$[0_{3\times1}]$	$\dots$	$[\tilde{\boldsymbol{r}}_{S_{c_N}/S_N}]\hat{\boldsymbol{s}}_N$	$\hat{\boldsymbol{s}}_N$

$$m_{\mathrm{sc}} = \sum_{i=0}^{N} m_{\mathrm{S}_i} \tag{34a}$$

$$m_{\mathrm{sc}} \boldsymbol{c} = \sum_{i=0}^{N} m_{\mathrm{S}_i} \boldsymbol{r}_{S_{c_i}/B} \tag{34b}$$

$$m_{\mathrm{sc}} \boldsymbol{c}' = \sum_{i=0}^{N} m_{\mathrm{S}_i} \boldsymbol{r}'_{S_{c_i}/B} \tag{34c}$$

$$m_{\mathrm{sc}} [\tilde{\boldsymbol{c}}] = \sum_{i=0}^{N} m_{\mathrm{S}_i} [\tilde{\boldsymbol{r}}_{S_{c_i}/B}] \tag{34d}$$

Substituting the equalities described above into Eq. (33), the compact form of the translational equation of motion is given by

$$\begin{aligned} &m_{\mathrm{sc}} \ddot{\boldsymbol{r}}_{B/N} - m_{\mathrm{sc}}[\tilde{\boldsymbol{c}}]\dot{\boldsymbol{\omega}}_{\mathcal{B}/\mathcal{N}} - \sum_{i=1}^{N}\left(\sum_{j=i}^{N} m_{\mathrm{S}_j}[\tilde{\boldsymbol{r}}_{S_{c_j}/S_i}]\right)\hat{\boldsymbol{s}}_i\ddot{\theta}_i \\ &\quad = \boldsymbol{F}_{\mathrm{ext}} - 2m_{\mathrm{sc}}[\tilde{\boldsymbol{\omega}}_{\mathcal{B}/\mathcal{N}}]\boldsymbol{c}' - m_{\mathrm{sc}}[\tilde{\boldsymbol{\omega}}_{\mathcal{B}/\mathcal{N}}][\tilde{\boldsymbol{\omega}}_{\mathcal{B}/\mathcal{N}}]\boldsymbol{c} \\ &\qquad - \sum_{i=1}^{N} m_{\mathrm{S}_i}\left(\sum_{j=1}^{i}[\tilde{\boldsymbol{\omega}}_{\mathcal{S}_j/\mathcal{S}_{j-1}}]\boldsymbol{r}'_{S_{c_i}/S_j} - \sum_{j=1}^{i-1}[\tilde{\boldsymbol{r}}_{S_{c_i}/S_{j+1}}][\tilde{\boldsymbol{\omega}}_{\mathcal{S}_j/\mathcal{B}}]\boldsymbol{\omega}_{\mathcal{S}_{j+1}/\mathcal{S}_j}\right) \end{aligned} \tag{35}$$

B. Rotational Equation of Motion

The rotational equation of motion determines the system's attitude history. For the rotational equation of motion, the generalized active force corresponds to the applied torque $\boldsymbol{F}_{4\text{–}6} = \boldsymbol{L}_B$, where $\boldsymbol{L}_B$ is the pure torque applied to the origin of the $\mathcal{B}$ frame. The generalized inertia force is

$$\begin{aligned} \boldsymbol{F}^*_{4\text{–}6} = &-\sum_{i=0}^{N}(m_{\mathrm{S}_i}[\boldsymbol{v}^{\mathcal{S}_{c_i}}_{4\text{–}6}]^T \ddot{\boldsymbol{r}}_{S_{c_i}/N} + [\boldsymbol{\omega}^{\mathcal{S}_i}_{4\text{–}6})]^T([I_{\mathrm{S}_i,S_{c_i}}]\dot{\boldsymbol{\omega}}_{\mathcal{S}_i/\mathcal{N}} \\ &+ [\tilde{\boldsymbol{\omega}}_{\mathcal{S}_i/\mathcal{N}}][I_{\mathrm{S}_i,S_{c_i}}]\boldsymbol{\omega}_{\mathcal{S}_i/\mathcal{N}})) \end{aligned} \tag{36}$$

It is important to note that none of the partial velocities are zero here, which means that all terms are accounted for. Kane's equation $\boldsymbol{F}_{4\text{–}6} + \boldsymbol{F}^*_{4\text{–}6} = \boldsymbol{0}$ is used:

$$\begin{aligned} &\boldsymbol{L}_B - \sum_{i=0}^{N} m_{\mathrm{S}_i}[\tilde{\boldsymbol{r}}_{S_{c_i}/B}]\ddot{\boldsymbol{r}}_{S_{c_i}/N} - \sum_{i=0}^{N}[I_{\mathrm{S}_i,S_{c_i}}]\dot{\boldsymbol{\omega}}_{\mathcal{S}_i/\mathcal{N}} \\ &\quad - \sum_{i=0}^{N}[\tilde{\boldsymbol{\omega}}_{\mathcal{S}_i/\mathcal{N}}][I_{\mathrm{S}_i,S_{c_i}}]\boldsymbol{\omega}_{\mathcal{S}_i/\mathcal{N}} = \boldsymbol{0} \end{aligned} \tag{37}$$

To simplify the equation above, the last term is expanded as follows:

$$\begin{aligned} &\sum_{i=0}^{N}[\tilde{\boldsymbol{\omega}}_{\mathcal{S}_i/\mathcal{N}}][I_{\mathrm{S}_i,S_{c_i}}]\boldsymbol{\omega}_{\mathcal{S}_i/\mathcal{N}} \\ &\quad = [\tilde{\boldsymbol{\omega}}_{\mathcal{B}/\mathcal{N}}]\left(\sum_{i=0}^{N}[I_{\mathrm{S}_i,S_{c_i}}]\right)\boldsymbol{\omega}_{\mathcal{B}/\mathcal{N}} + \left(\sum_{i=0}^{N}[\tilde{\boldsymbol{\omega}}_{\mathcal{S}_i/\mathcal{B}}][I_{\mathrm{S}_i,S_{c_i}}]\right)\boldsymbol{\omega}_{\mathcal{B}/\mathcal{N}} \\ &\qquad + \sum_{i=0}^{N}[\tilde{\boldsymbol{\omega}}_{\mathcal{S}_i/\mathcal{N}}][I_{\mathrm{S}_i,S_{c_i}}]\boldsymbol{\omega}_{\mathcal{S}_i/\mathcal{B}} \end{aligned} \tag{38}$$

Moreover, the triple cross product identity $\boldsymbol{a}\times(\boldsymbol{b}\times\boldsymbol{c}) = -\boldsymbol{c}\times(\boldsymbol{a}\times\boldsymbol{b}) + \boldsymbol{b}\times(\boldsymbol{a}\times\boldsymbol{c})$ is used to get the following equalities:

$$[\tilde{\boldsymbol{r}}_{S_{c_i}/B}][\tilde{\boldsymbol{\omega}}_{\mathcal{B}/\mathcal{N}}][\tilde{\boldsymbol{\omega}}_{\mathcal{B}/\mathcal{N}}]\boldsymbol{r}_{S_{c_i}/B} = -[\tilde{\boldsymbol{\omega}}_{\mathcal{B}/\mathcal{N}}][\tilde{\boldsymbol{r}}_{S_{c_i}/B}][\tilde{\boldsymbol{r}}_{S_{c_i}/B}]\boldsymbol{\omega}_{\mathcal{B}/\mathcal{N}} \tag{39}$$

$$[\tilde{\boldsymbol{r}}_{S_{c_i}/B}][\tilde{\boldsymbol{\omega}}_{\mathcal{B}/\mathcal{N}}]\boldsymbol{r}'_{S_{c_i}/B} = -[\tilde{\boldsymbol{r}}'_{S_{c_i}/B}][\tilde{\boldsymbol{r}}_{S_{c_i}/B}]\boldsymbol{\omega}_{\mathcal{B}/\mathcal{N}} + [\tilde{\boldsymbol{\omega}}_{\mathcal{B}/\mathcal{N}}][\tilde{\boldsymbol{r}}_{S_{c_i}/B}]\boldsymbol{r}'_{S_{c_i}/B} \tag{40}$$

These are used to group like terms and to bring the equation into its final form. Expanding the acceleration terms and plugging these results into Eq. (37) yields

$$\begin{aligned} &\sum_{i=0}^{N} m_{\mathrm{S}_i}[\tilde{\boldsymbol{r}}_{S_{c_i}/B}]\ddot{\boldsymbol{r}}_{B/N} + \sum_{i=0}^{N}([I_{\mathrm{S}_i,S_{c_i}}] - m_{\mathrm{S}_i}[\tilde{\boldsymbol{r}}_{S_{c_i}/B}][\tilde{\boldsymbol{r}}_{S_{c_i}/B}])\dot{\boldsymbol{\omega}}_{\mathcal{B}/\mathcal{N}} \\ &\quad + \sum_{i=1}^{N}\sum_{j=1}^{i}([I_{\mathrm{S}_i,S_{c_i}}] - m_{\mathrm{S}_i}[\tilde{\boldsymbol{r}}_{S_{c_i}/B}][\tilde{\boldsymbol{r}}_{S_{c_i}/S_j}])\hat{\boldsymbol{s}}_j\ddot{\theta}_j \\ &\quad = \boldsymbol{L}_B - [\tilde{\boldsymbol{\omega}}_{\mathcal{B}/\mathcal{N}}]\sum_{i=0}^{N}([I_{\mathrm{S}_i,S_{c_i}}] - m_{\mathrm{S}_i}[\tilde{\boldsymbol{r}}_{S_{c_i}/B}][\tilde{\boldsymbol{r}}_{S_{c_i}/B}])\boldsymbol{\omega}_{\mathcal{B}/\mathcal{N}} \\ &\qquad - \sum_{i=0}^{N}([\tilde{\boldsymbol{\omega}}_{\mathcal{S}_i/\mathcal{B}}][I_{\mathrm{S}_i,S_{c_i}}] - [I_{\mathrm{S}_i,S_{c_i}}][\tilde{\boldsymbol{\omega}}_{\mathcal{S}_i/\mathcal{B}}] \\ &\qquad - m_{\mathrm{S}_i}([\tilde{\boldsymbol{r}}_{S_{c_i}/B}][\tilde{\boldsymbol{r}}'_{S_{c_i}/B}] + [\tilde{\boldsymbol{r}}'_{S_{c_i}/B}][\tilde{\boldsymbol{r}}_{S_{c_i}/B}]))\boldsymbol{\omega}_{\mathcal{B}/\mathcal{N}} \\ &\qquad - \sum_{i=1}^{N}\Bigg([\tilde{\boldsymbol{\omega}}_{\mathcal{S}_i/\mathcal{N}}][I_{\mathrm{S}_i,S_{c_i}}]\boldsymbol{\omega}_{\mathcal{S}_i/\mathcal{B}} - [I_{\mathrm{S}_i,S_{c_i}}]\sum_{j=1}^{i-1}[\tilde{\boldsymbol{\omega}}_{\mathcal{S}_i/\mathcal{S}_j}]\boldsymbol{\omega}_{\mathcal{S}_j/\mathcal{S}_{j-1}} \\ &\qquad + m_{\mathrm{S}_i}[\tilde{\boldsymbol{\omega}}_{\mathcal{B}/\mathcal{N}}][\tilde{\boldsymbol{r}}_{S_{c_i}/B}]\boldsymbol{r}'_{S_{c_i}/B}\Bigg) \\ &\qquad - \sum_{i=1}^{N} m_{\mathrm{S}_i}[\tilde{\boldsymbol{r}}_{S_{c_i}/B}]\Bigg(\sum_{j=1}^{i}[\tilde{\boldsymbol{\omega}}_{\mathcal{S}_j/\mathcal{S}_{j-1}}]\boldsymbol{r}'_{S_{c_i}/S_j} \\ &\qquad - \sum_{j=1}^{i-1}[\tilde{\boldsymbol{r}}_{S_{c_i}/S_{j+1}}][\tilde{\boldsymbol{\omega}}_{\mathcal{S}_j/\mathcal{B}}]\boldsymbol{\omega}_{\mathcal{S}_{j+1}/\mathcal{S}_j}\Bigg) \end{aligned} \tag{41}$$

Once again, all explicit second-order acceleration terms are grouped on the left-hand side to ensure that this analytical solution is suitable for the BSM formulation. The following system inertia definitions are useful:

$$[I_{\mathrm{sc},B}] = \sum_{i=0}^{N}([I_{\mathrm{S}_i,S_{c_i}}] - m_{\mathrm{S}_i}[\tilde{\boldsymbol{r}}_{S_{c_i}/B}][\tilde{\boldsymbol{r}}_{S_{c_i}/B}]) \tag{42}$$

$$\begin{aligned} [I'_{\mathrm{sc},B}] = &\sum_{i=0}^{N}([\tilde{\boldsymbol{\omega}}_{\mathcal{S}_i/\mathcal{B}}][I_{\mathrm{S}_i,S_{c_i}}] - [I_{\mathrm{S}_i,S_{c_i}}][\tilde{\boldsymbol{\omega}}_{\mathcal{S}_i/\mathcal{B}}] \\ &- m_{\mathrm{S}_i}([\tilde{\boldsymbol{r}}_{S_{c_i}/B}][\tilde{\boldsymbol{r}}'_{S_{c_i}/B}] + [\tilde{\boldsymbol{r}}'_{S_{c_i}/B}][\tilde{\boldsymbol{r}}_{S_{c_i}/B}])) \end{aligned} \tag{43}$$

The equation of motion above is simplified to show the compact form of the rotational equation of motion:

$$\begin{aligned} &m_{\mathrm{sc}}[\tilde{\boldsymbol{c}}]\ddot{\boldsymbol{r}}_{B/N} + [I_{\mathrm{sc},B}]\dot{\boldsymbol{\omega}}_{\mathcal{B}/\mathcal{N}} \\ &\quad + \sum_{i=1}^{N}\left(\sum_{j=i}^{N}([I_{\mathrm{S}_j,S_{c_j}}] - m_{\mathrm{S}_j}[\tilde{\boldsymbol{r}}_{S_{c_j}/B}][\tilde{\boldsymbol{r}}_{S_{c_j}/S_i}])\right)\hat{\boldsymbol{s}}_i\ddot{\theta}_i \\ &\quad = \boldsymbol{L}_B - [\tilde{\boldsymbol{\omega}}_{\mathcal{B}/\mathcal{N}}][I_{\mathrm{sc},B}]\boldsymbol{\omega}_{\mathcal{B}/\mathcal{N}} - [I'_{\mathrm{sc},B}]\boldsymbol{\omega}_{\mathcal{B}/\mathcal{N}} \\ &\quad - \sum_{i=1}^{N}\Bigg([\tilde{\boldsymbol{\omega}}_{\mathcal{S}_i/\mathcal{N}}][I_{\mathrm{S}_i,S_{c_i}}]\boldsymbol{\omega}_{\mathcal{S}_i/\mathcal{B}} - [I_{\mathrm{S}_i,S_{c_i}}]\sum_{j=1}^{i-1}[\tilde{\boldsymbol{\omega}}_{\mathcal{S}_i/\mathcal{S}_j}]\boldsymbol{\omega}_{\mathcal{S}_j/\mathcal{S}_{j-1}} \\ &\quad + m_{\mathrm{S}_i}[\tilde{\boldsymbol{\omega}}_{\mathcal{B}/\mathcal{N}}][\tilde{\boldsymbol{r}}_{S_{c_i}/B}]\boldsymbol{r}'_{S_{c_i}/B}\Bigg) - \sum_{i=1}^{N} m_{\mathrm{S}_i}[\tilde{\boldsymbol{r}}_{S_{c_i}/B}]\Bigg(\sum_{j=1}^{i}[\tilde{\boldsymbol{\omega}}_{\mathcal{S}_j/\mathcal{S}_{j-1}}]\boldsymbol{r}'_{S_{c_i}/S_j} \\ &\quad - \sum_{j=1}^{i-1}[\tilde{\boldsymbol{r}}_{S_{c_i}/S_{j+1}}][\tilde{\boldsymbol{\omega}}_{\mathcal{S}_j/\mathcal{B}}]\boldsymbol{\omega}_{\mathcal{S}_{j+1}/\mathcal{S}_j}\Bigg) \end{aligned} \tag{44}$$

C. Equation of Motion of *n*-th Spinning Body

This section aims to find the equation for each row of the matrix equation in Eq. (10). For the *n*th equation of motion, the generalized active force is $F_n = u_n$ and the generalized inertia force is

$$F_n^* = -\sum_{i=n}^{N}(m_{\mathrm{S}_i}[\boldsymbol{v}_n^{S_{c_i}}]^T \ddot{\boldsymbol{r}}_{S_{c_i}/N} + [\boldsymbol{\omega}_n^{S_i}]^T([I_{\mathrm{S}_i,S_{c_i}}]\dot{\boldsymbol{\omega}}_{\mathcal{S}_i/\mathcal{N}} + [\tilde{\boldsymbol{\omega}}_{\mathcal{S}_i/\mathcal{N}}][I_{\mathrm{S}_i,S_{c_i}}]\boldsymbol{\omega}_{\mathcal{S}_i/\mathcal{N}})) \tag{45}$$

where, using the partial velocity table, $[\boldsymbol{v}_n^{S_{c_i}}] = [\tilde{\boldsymbol{r}}_{S_{c_i}/S_n}]\hat{\boldsymbol{s}}_n$ and $[\boldsymbol{\omega}_n^{S_i}] = \hat{\boldsymbol{s}}_n$. Kane's equation $F_n + F_n^* = 0$ is used to get

$$\begin{aligned}
&\hat{\boldsymbol{s}}_n^T \sum_{i=n}^{N}\sum_{j=1}^{i}([I_{\mathrm{S}_i,S_{c_i}}] - m_{\mathrm{S}_i}[\tilde{\boldsymbol{r}}_{S_{c_i}/S_n}][\tilde{\boldsymbol{r}}_{S_{c_i}/S_j}])\hat{\boldsymbol{s}}_j\ddot{\theta}_j \\
&= u_n - \hat{\boldsymbol{s}}_n^T \sum_{i=n}^{N} m_{\mathrm{S}_i}[\tilde{\boldsymbol{r}}_{S_{c_i}/S_n}]\ddot{\boldsymbol{r}}_{B/N} - \hat{\boldsymbol{s}}_n^T \sum_{i=n}^{N}([I_{\mathrm{S}_i,S_{c_i}}] \\
&\quad - m_{\mathrm{S}_i}[\tilde{\boldsymbol{r}}_{S_{c_i}/S_n}][\tilde{\boldsymbol{r}}_{S_{c_i}/B}])\dot{\boldsymbol{\omega}}_{\mathcal{B}/\mathcal{N}} \\
&\quad - \hat{\boldsymbol{s}}_n^T \sum_{i=n}^{N}\Bigg([\tilde{\boldsymbol{\omega}}_{\mathcal{S}_i/\mathcal{N}}][I_{\mathrm{S}_i,S_{c_i}}]\boldsymbol{\omega}_{\mathcal{S}_i/\mathcal{N}} - [I_{\mathrm{S}_i,S_{c_i}}][\tilde{\boldsymbol{\omega}}_{\mathcal{S}_i/\mathcal{B}}]\boldsymbol{\omega}_{\mathcal{B}/\mathcal{N}} \\
&\quad - [I_{\mathrm{S}_i,S_{c_i}}]\sum_{j=1}^{i-1}[\tilde{\boldsymbol{\omega}}_{\mathcal{S}_i/\mathcal{S}_j}]\boldsymbol{\omega}_{\mathcal{S}_j/\mathcal{S}_{j-1}}\Bigg) \\
&\quad - \hat{\boldsymbol{s}}_n^T \sum_{i=n}^{N} m_{\mathrm{S}_i}[\tilde{\boldsymbol{r}}_{S_{c_i}/S_n}]\Bigg([\tilde{\boldsymbol{\omega}}_{\mathcal{B}/\mathcal{N}}][\tilde{\boldsymbol{\omega}}_{\mathcal{B}/\mathcal{N}}]\boldsymbol{r}_{S_{c_i}/B} + 2[\tilde{\boldsymbol{\omega}}_{\mathcal{B}/\mathcal{N}}]\boldsymbol{r}'_{S_{c_i}/B} \\
&\quad + \sum_{j=1}^{i}[\tilde{\boldsymbol{\omega}}_{\mathcal{S}_j/\mathcal{S}_{j-1}}]\boldsymbol{r}'_{S_{c_i}/S_j} - \sum_{j=1}^{i-1}[\tilde{\boldsymbol{r}}_{S_{c_i}/S_{j+1}}][\tilde{\boldsymbol{\omega}}_{\mathcal{S}_j/\mathcal{B}}]\boldsymbol{\omega}_{\mathcal{S}_{j+1}/\mathcal{S}_j}\Bigg)
\end{aligned} \tag{46}$$

Note that the state acceleration is moved to the left, while all other terms are on the right. Moreover, $\ddot{\boldsymbol{r}}_{B/N}$ and $\dot{\boldsymbol{\omega}}_{\mathcal{B}/\mathcal{N}}$ are explicitly written, and every other term consists of additional contributions that do not explicitly depend on state accelerations. As usual, it is convenient to rewrite the double summation in $\hat{\boldsymbol{s}}_j\ddot{\theta}_j$ using Eq. (59), which yields the alternative form:

$$\begin{aligned}
&\hat{\boldsymbol{s}}_n^T \sum_{i=1}^{n}\left(\sum_{j=n}^{N}([I_{\mathrm{S}_j,S_{c_j}}] - m_{\mathrm{S}_j}[\tilde{\boldsymbol{r}}_{S_{c_j}/S_n}][\tilde{\boldsymbol{r}}_{S_{c_j}/S_i}])\right)\hat{\boldsymbol{s}}_i\ddot{\theta}_i \\
&\quad + \hat{\boldsymbol{s}}_n^T \sum_{i=n+1}^{N}\left(\sum_{j=i}^{N}([I_{\mathrm{S}_j,S_{c_j}}] - m_{\mathrm{S}_j}[\tilde{\boldsymbol{r}}_{S_{c_j}/S_n}][\tilde{\boldsymbol{r}}_{S_{c_j}/S_i}])\right)\hat{\boldsymbol{s}}_i\ddot{\theta}_i \\
&= u_n - \hat{\boldsymbol{s}}_n^T \sum_{i=n}^{N} m_{\mathrm{S}_i}[\tilde{\boldsymbol{r}}_{S_{c_i}/S_n}]\ddot{\boldsymbol{r}}_{B/N} - \hat{\boldsymbol{s}}_n^T \sum_{i=n}^{N}([I_{\mathrm{S}_i,S_{c_i}}] \\
&\quad - m_{\mathrm{S}_i}[\tilde{\boldsymbol{r}}_{S_{c_i}/S_n}][\tilde{\boldsymbol{r}}_{S_{c_i}/B}])\dot{\boldsymbol{\omega}}_{\mathcal{B}/\mathcal{N}} \\
&\quad - \hat{\boldsymbol{s}}_n^T \sum_{i=n}^{N}\Bigg([\tilde{\boldsymbol{\omega}}_{\mathcal{S}_i/\mathcal{N}}][I_{\mathrm{S}_i,S_{c_i}}]\boldsymbol{\omega}_{\mathcal{S}_i/\mathcal{N}} - [I_{\mathrm{S}_i,S_{c_i}}][\tilde{\boldsymbol{\omega}}_{\mathcal{S}_i/\mathcal{B}}]\boldsymbol{\omega}_{\mathcal{B}/\mathcal{N}} \\
&\quad - [I_{\mathrm{S}_i,S_{c_i}}]\sum_{j=1}^{i-1}[\tilde{\boldsymbol{\omega}}_{\mathcal{S}_i/\mathcal{S}_j}]\boldsymbol{\omega}_{\mathcal{S}_j/\mathcal{S}_{j-1}}\Bigg) \\
&\quad - \hat{\boldsymbol{s}}_n^T \sum_{i=n}^{N} m_{\mathrm{S}_i}[\tilde{\boldsymbol{r}}_{S_{c_i}/S_n}]\Bigg([\tilde{\boldsymbol{\omega}}_{\mathcal{B}/\mathcal{N}}][\tilde{\boldsymbol{\omega}}_{\mathcal{B}/\mathcal{N}}]\boldsymbol{r}_{S_{c_i}/B} + 2[\tilde{\boldsymbol{\omega}}_{\mathcal{B}/\mathcal{N}}]\boldsymbol{r}'_{S_{c_i}/B} \\
&\quad + \sum_{j=1}^{i}[\tilde{\boldsymbol{\omega}}_{\mathcal{S}_j/\mathcal{S}_{j-1}}]\boldsymbol{r}'_{S_{c_i}/S_j} - \sum_{j=1}^{i-1}[\tilde{\boldsymbol{r}}_{S_{c_i}/S_{j+1}}][\tilde{\boldsymbol{\omega}}_{\mathcal{S}_j/\mathcal{B}}]\boldsymbol{\omega}_{\mathcal{S}_{j+1}/\mathcal{S}_j}\Bigg)
\end{aligned} \tag{47}$$

This is the compact form of the effector equation of motion for the nth degree of freedom. Notice how using the double-summation property yields two different summations in $\hat{\boldsymbol{s}}_j\ddot{\theta}_j$, as shown in Appendix A, which has implications when building the effector's mass matrix.

D. Backsubstitution Formulation

Let us define each term introduced in the equations above for the problem at hand. First, the terms in Eq. (10) are defined. The element of the mass matrix in the nth row and ith column is defined as

$$\boldsymbol{M}_{\theta_{n,i}} = \begin{cases} \hat{\boldsymbol{s}}_n^T \sum_{j=n}^{N}([I_{\mathrm{S}_j,S_{c_j}}] - m_{\mathrm{S}_j}[\tilde{\boldsymbol{r}}_{S_{c_j}/S_n}][\tilde{\boldsymbol{r}}_{S_{c_j}/S_i}])\hat{\boldsymbol{s}}_i, & i \le n \\ \hat{\boldsymbol{s}}_n^T \sum_{j=i}^{N}([I_{\mathrm{S}_j,S_{c_j}}] - m_{\mathrm{S}_j}[\tilde{\boldsymbol{r}}_{S_{c_j}/S_n}][\tilde{\boldsymbol{r}}_{S_{c_j}/S_i}])\hat{\boldsymbol{s}}_i, & i > n \end{cases} \tag{48}$$

The two summations from Eq. (47) are clear in the definition of the effector mass matrix. Each entry depends on whether n is greater or smaller than i. The other terms are defined nth rowwise as

$$\boldsymbol{A}^*_{\theta_n} = -\hat{\boldsymbol{s}}_n^T \sum_{i=n}^{N} m_{\mathrm{S}_i}[\tilde{\boldsymbol{r}}_{S_{c_i}/S_n}] \tag{49}$$

$$\boldsymbol{B}^*_{\theta_n} = -\hat{\boldsymbol{s}}_n^T \sum_{i=n}^{N}([I_{\mathrm{S}_i,S_{c_i}}] - m_{\mathrm{S}_i}[\tilde{\boldsymbol{r}}_{S_{c_i}/S_n}][\tilde{\boldsymbol{r}}_{S_{c_i}/B}]) \tag{50}$$

$$\begin{aligned}
\boldsymbol{C}^*_{\theta_n} &= u_n - \hat{\boldsymbol{s}}_n^T \sum_{i=n}^{N}\Bigg([\tilde{\boldsymbol{\omega}}_{\mathcal{S}_i/\mathcal{N}}][I_{\mathrm{S}_i,S_{c_i}}]\boldsymbol{\omega}_{\mathcal{S}_i/\mathcal{N}} - [I_{\mathrm{S}_i,S_{c_i}}][\tilde{\boldsymbol{\omega}}_{\mathcal{S}_i/\mathcal{B}}]\boldsymbol{\omega}_{\mathcal{B}/\mathcal{N}} \\
&\quad - [I_{\mathrm{S}_i,S_{c_i}}]\sum_{j=1}^{i-1}[\tilde{\boldsymbol{\omega}}_{\mathcal{S}_i/\mathcal{S}_j}]\boldsymbol{\omega}_{\mathcal{S}_j/\mathcal{S}_{j-1}} \\
&\quad + m_{\mathrm{S}_i}[\tilde{\boldsymbol{r}}_{S_{c_i}/S_n}]\Bigg([\tilde{\boldsymbol{\omega}}_{\mathcal{B}/\mathcal{N}}][\tilde{\boldsymbol{\omega}}_{\mathcal{B}/\mathcal{N}}]\boldsymbol{r}_{S_{c_i}/B} + 2[\tilde{\boldsymbol{\omega}}_{\mathcal{B}/\mathcal{N}}]\boldsymbol{r}'_{S_{c_i}/B} \\
&\quad + \sum_{j=1}^{i}[\tilde{\boldsymbol{\omega}}_{\mathcal{S}_j/\mathcal{S}_{j-1}}]\boldsymbol{r}'_{S_{c_i}/S_j} - \sum_{j=1}^{i-1}[\tilde{\boldsymbol{r}}_{S_{c_i}/S_{j+1}}][\tilde{\boldsymbol{\omega}}_{\mathcal{S}_j/\mathcal{B}}]\boldsymbol{\omega}_{\mathcal{S}_{j+1}/\mathcal{S}_j}\Bigg)\Bigg)
\end{aligned} \tag{51}$$

With the effector equation terms defined, the terms for solving the translational and rotational acceleration can be found. The matrices for this problem are given by

$$[A] = m_{\mathrm{sc}}[I_{3\times 3}] - \sum_{i=1}^{N}\left(\sum_{j=i}^{N} m_{\mathrm{S}_j}[\tilde{\boldsymbol{r}}_{S_{c_j}/S_i}]\right)\hat{\boldsymbol{s}}_i\boldsymbol{A}_{\theta_i} \tag{52}$$

$$[B] = -m_{\mathrm{sc}}[\tilde{\boldsymbol{c}}] - \sum_{i=1}^{N}\left(\sum_{j=i}^{N} m_{\mathrm{S}_j}[\tilde{\boldsymbol{r}}_{S_{c_j}/S_i}]\right)\hat{\boldsymbol{s}}_i\boldsymbol{B}_{\theta_i} \tag{53}$$

$$[C] = m_{\mathrm{sc}}[\tilde{\boldsymbol{c}}] + \sum_{i=1}^{N}\left(\sum_{j=i}^{N}([I_{\mathrm{S}_j,S_{c_j}}] - m_{\mathrm{S}_j}[\tilde{\boldsymbol{r}}_{S_{c_j}/B}][\tilde{\boldsymbol{r}}_{S_{c_j}/S_i}])\right)\hat{\boldsymbol{s}}_i\boldsymbol{A}_{\theta_i} \tag{54}$$

$$[D] = [I_{\mathrm{sc},B}] + \sum_{i=1}^{N}\left(\sum_{j=i}^{N}([I_{\mathrm{S}_j,S_{c_j}}] - m_{\mathrm{S}_j}[\tilde{\boldsymbol{r}}_{S_{c_j}/B}][\tilde{\boldsymbol{r}}_{S_{c_j}/S_i}])\right)\hat{\boldsymbol{s}}_i\boldsymbol{B}_{\theta_i} \tag{55}$$

Notice how the $\boldsymbol{A}_{\theta_i}$ and $\boldsymbol{B}_{\theta_i}$ terms are used instead of $\boldsymbol{A}^*_{\theta_i}$ and $\boldsymbol{B}^*_{\theta_i}$. The latter are defined directly from the equations of motion of each spinning body but cannot be used directly. The effector mass matrix must be inverted, resulting in the former terms that cannot be defined analytically. The additional translational and rotational contributions are

$$\begin{aligned}
\boldsymbol{v}_{\mathrm{Trans}} &= \boldsymbol{F}_{\mathrm{ext}} - 2m_{\mathrm{sc}}[\tilde{\boldsymbol{\omega}}_{\mathcal{B}/\mathcal{N}}]\boldsymbol{c}' - m_{\mathrm{sc}}[\tilde{\boldsymbol{\omega}}_{\mathcal{B}/\mathcal{N}}][\tilde{\boldsymbol{\omega}}_{\mathcal{B}/\mathcal{N}}]\boldsymbol{c} \\
&\quad - \sum_{i=1}^{N} m_{\mathrm{S}_i}\left(\sum_{j=1}^{i}[\tilde{\boldsymbol{\omega}}_{\mathcal{S}_j/\mathcal{S}_{j-1}}]\boldsymbol{r}'_{S_{c_i}/S_j} - \sum_{j=1}^{i-1}[\tilde{\boldsymbol{r}}_{S_{c_i}/S_{j+1}}][\tilde{\boldsymbol{\omega}}_{\mathcal{S}_j/\mathcal{B}}]\boldsymbol{\omega}_{\mathcal{S}_{j+1}/\mathcal{S}_j}\right) \\
&\quad + \sum_{i=1}^{N}\left(\sum_{j=i}^{N} m_{\mathrm{S}_j}[\tilde{\boldsymbol{r}}_{S_{c_j}/S_i}]\right)\hat{\boldsymbol{s}}_i\boldsymbol{C}_{\theta_i}
\end{aligned} \tag{56}$$

$$
\begin{aligned}
\boldsymbol{v}_{\mathrm{Rot}} = {} & \boldsymbol{L}_B - [\tilde{\boldsymbol{\omega}}_{\mathcal{B}/\mathcal{N}}][I_{\mathrm{sc},B}]\boldsymbol{\omega}_{\mathcal{B}/\mathcal{N}} - [I'_{\mathrm{sc},B}]\boldsymbol{\omega}_{\mathcal{B}/\mathcal{N}} \\
& - \sum_{i=1}^{N}\Bigg([\tilde{\boldsymbol{\omega}}_{\mathcal{S}_i/\mathcal{N}}][I_{\mathrm{S}_i,S_{c_i}}]\boldsymbol{\omega}_{\mathcal{S}_i/\mathcal{B}} - [I_{\mathrm{S}_i,S_{c_i}}]\sum_{j=1}^{i-1}[\tilde{\boldsymbol{\omega}}_{\mathcal{S}_i/\mathcal{S}_j}]\boldsymbol{\omega}_{\mathcal{S}_j/\mathcal{S}_{j-1}} \\
& + m_{\mathrm{S}_i}[\tilde{\boldsymbol{\omega}}_{\mathcal{B}/\mathcal{N}}][\tilde{\boldsymbol{r}}_{S_{c_i}/B}]\boldsymbol{r}'_{S_{c_i}/B}\Bigg) \\
& - \sum_{i=1}^{N} m_{\mathrm{S}_i}[\tilde{\boldsymbol{r}}_{S_{c_i}/B}]\Bigg(\sum_{j=1}^{i}[\tilde{\boldsymbol{\omega}}_{\mathcal{S}_j/\mathcal{S}_{j-1}}]\boldsymbol{r}'_{S_{c_i}/S_j} \\
& - \sum_{j=1}^{i-1}[\tilde{\boldsymbol{r}}_{S_{c_i}/S_{j+1}}][\tilde{\boldsymbol{\omega}}_{\mathcal{S}_j/\mathcal{B}}]\boldsymbol{\omega}_{\mathcal{S}_{j+1}/\mathcal{S}_j}\Bigg) \\
& - \sum_{i=1}^{N}\Bigg(\sum_{j=i}^{N}([I_{\mathrm{S}_j,S_{c_j}}] - m_{\mathrm{S}_j}[\tilde{\boldsymbol{r}}_{S_{c_j}/B}][\tilde{\boldsymbol{r}}_{S_{c_j}/S_i}])\Bigg)\hat{\boldsymbol{s}}_i\boldsymbol{C}_{\theta_i}
\end{aligned}
\tag{57}
$$

VI. Numerical Example

This section provides a practical example of using the N-axis effector. It aims to demonstrate two applications supported by the same software architecture and equations. The general N-body sequential spinner effector presented is implemented in the open-source Basilisk[¶] simulation framework [35], which uses the BSM formulation [20] as its dynamics engine. The documentation for the effector can be found online.[***]

The first scenario uses the effector as a robotic arm. The robotic arm comprises two links, each capable of rotating about two axes. The second scenario shows the effector being used to approximate a flexible panel. The panel is discretized into multiple subpanels, each of which has bending and torsional modes. The hub parameters used in both simulations are shown in Table 3.

The initial conditions for both simulations are identical and are shown in Table 4.

A. Robotic Arm Simulation

The first scenario simulates a spacecraft with a rigid hub and a robotic arm attached, orbiting Earth. The goal of this scenario is to demonstrate the fully coupled motion of a representative component, specifically a two-arm, four-degree-of-freedom arm that could be attached to a spacecraft for various applications. The full simulation software for the robotic arm scenario is implemented in the open-source Basilisk simulation framework and is publicly available as an example scenario.[†††] The scenario documentation contains a video illustration of the resulting spacecraft motion.[‡‡‡] A diagram of the spacecraft is shown in Fig. 8. The system starts at rest, and the robotic arm then pivots from its nominal initial position to a final set of angles, with the hub responding accordingly.

The robotic arm is modeled as two cylindrical links with a diameter of 0.6 m and a height of 3 m. Each link pivots about its pitch and roll axes. Each link is commanded by a rotational spring-damper that tracks a specified reference angle and angular rate. Additional mass properties are given in Table 5. The robotic arm is initialized at the nominal position (all angles and angle rates set to zero). The reference is provided by a profiler, which yields a reference path for both angle and angular rate. The final angles and angle rates for each degree of freedom are shown in Table 6. The profiler uses a maximum angular acceleration of 0.01 $\deg/\mathrm{s}^2$ for the first link and 0.02 $\deg/\mathrm{s}^2$ for the second, both smoothed over 10 s.

[¶]https://avslab.github.io/basilisk/index.html.
[***]https://avslab.github.io/basilisk/Documentation/simulation/dynamics/spinningBodies/spinningBodiesNDOF/spinningBodyNDOFStateEffector.html.
[†††]https://avslab.github.io/basilisk/examples/scenarioRoboticArm.html.
[‡‡‡]https://youtu.be/4mMCCTVHZkA.

Table 3 Simulation parameters for the rigid hub

Parameter	Notation	Value	Units
Hub's mass	m_{hub}	1000	kg
Hub's inertia about the hub's center of mass	${}^{\mathcal{B}}[I_{\mathrm{hub},B_c}]$	${}^{\mathcal{B}}\begin{bmatrix} 3750 & 0 & 0 \\ 0 & 3750 & 0 \\ 0 & 0 & 1500 \end{bmatrix}$	$\mathrm{kg}\cdot\mathrm{m}^2$
Hub's center-of-mass location with respect to B	${}^{\mathcal{B}}\boldsymbol{r}_{B_c/B}$	${}^{\mathcal{B}}[0,0,0]^T$	m

Table 4 Spacecraft initial conditions

Parameter	Notation	Value	Units
Semimajor axis	a	8000	km
Eccentricity	e	0.1	— —
Inclination	i	0	deg
Longitude of the ascending node	Ω	0	deg
Argument of periapsis	ω	0	deg
Initial true anomaly	f	0	deg

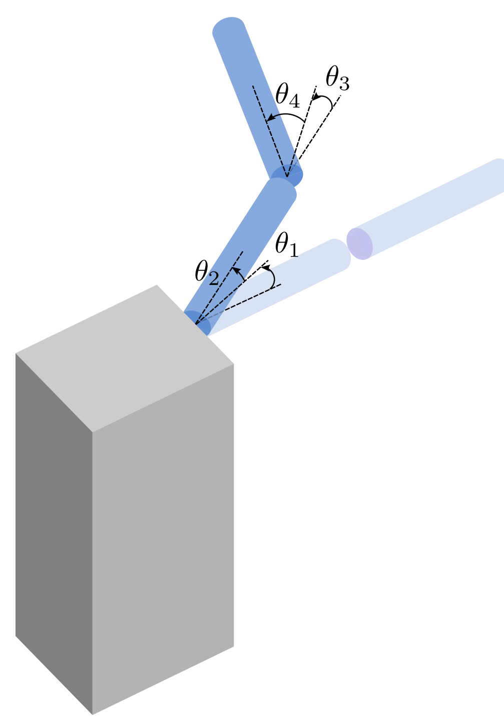

Fig. 8 Schematic of the spacecraft with a robotic arm. The lighter arm corresponds to the undeflected state.

The time history for all angles and angle rates is shown in Fig. 9. As expected, Fig. 9a shows that all angles start at zero, the nominal position, and then move to the final reference angles. Figure 9b shows the angle rates tracking the desired profile, indicating that the chosen spring and damper constants are high enough to track the moving reference. The slope for the first link's angle rates is half the slope of the second link's angle rates because of each profiler's maximum angular acceleration. Also, note the smoothing over a 10 s window around the transitions between acceleration and deceleration.

The time history for the hub's attitude, expressed in modified Rodrigues parameters [30], and angular velocity is shown in Fig. 10. Figure 10a shows the attitude of the hub. Because the hub and the robotic arm are fully coupled, the hub's attitude changes as the robotic arm moves along the profiled trajectory. This can also be

Table 5 Simulation parameters for the robotic arm simulation

Parameter	Notation	Value	Units
Link's mass	m_{S_i}	50	kg
Link's inertia about its center of mass	${}^{\mathcal{S}_i}[I_{S_i,S_{c_i}}]$	${}^{\mathcal{S}_i}\begin{bmatrix} 38.625 & 0 & 0 \\ 0 & 0.375 & 0 \\ 0 & 0 & 38.625 \end{bmatrix}$	$\text{kg} \cdot \text{m}^2$
Link's center-of-mass location with respect to hinge point	${}^{\mathcal{S}_i}\boldsymbol{r}_{S_{c_i}/S_i}$	${}^{\mathcal{S}_i}[0, 1.5, 0]^T$	m
Position between hinge points	${}^{\mathcal{S}_i}\boldsymbol{r}_{S_i/S_{i-1}}$	${}^{\mathcal{S}_i}[0, 3, 0]^T$	m
Pitch rotation axis	${}^{\mathcal{S}_i}\hat{s}_i$	${}^{\mathcal{S}_i}[1, 0, 0]^T$	— —
Yaw rotation axis	${}^{\mathcal{S}_i}\hat{s}_i$	${}^{\mathcal{S}_i}[0, 0, 1]^T$	— —
Linear spring constant	k_i	500	$\text{N} \cdot \text{m/rad}$
Linear damper constant	c_i	100	$\text{N} \cdot \text{m/rad}$

Table 6 Profiled final angle and angle rate for each degree of freedom

Degree of freedom	Reference final angle, deg	Reference final angle rate, deg/s
First link pitch	−30	0
First link yaw	45	0
Second link pitch	90	0
Second link yaw	−20	0

seen in Fig. 10b, which shows the angular velocity of the hub. Here, the angular velocity varies like that of the robotic links, as their coupling causes the hub to react opposite to the effector. Note that the end angular velocity is zero at the beginning and end, while the final attitude is not zero due to the configuration change. This behavior is a consequence of angular-momentum conservation. The profiled reference angle serves as an internal torque between the effector and the hub and does not affect the spacecraft's total angular momentum. Because the system starts with zero angular momentum, it ends with zero angular momentum when the effector stops moving.

B. Flexible Panel Scenario via Classical Lumped Finite-Body Approach

The second scenario simulates a spacecraft comprising a rigid hub with a highly flexible panel while orbiting Earth. The purpose of this flexible panel scenario is to demonstrate that the previously developed N-axis formulation can simulate first-order flexion of components. It is not intended to represent any real component, as the spring and damper coefficients are deliberately selected to induce large, unrealistic deformations. Rather, the goal is to demonstrate that

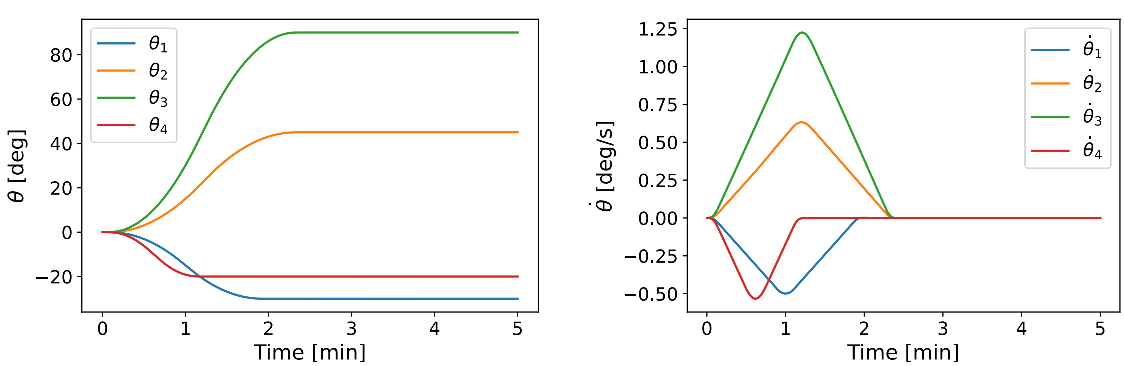

a) Effector angles

b) Effector angle rates

Fig. 9 Time history of all degrees of freedom of the robotic arm.

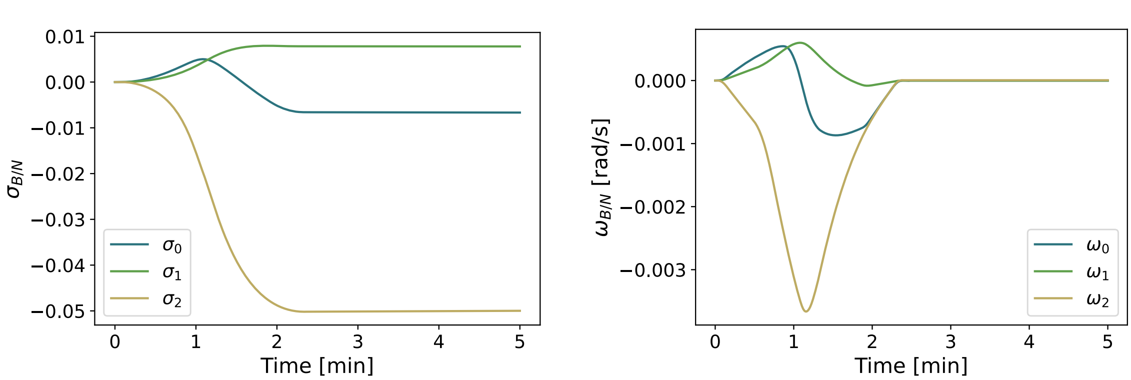

a) Attitude of the hub

b) Angular velocity of the hub

Fig. 10 Time history for the hub's states with a robotic arm.

Table 7 Simulation parameters for the flexible panel simulation

Parameter	Notation	Value	Units
Subpanel's mass	m_{S_i}	20	kg
Subpanel's inertia about its center of mass	${}^{S_1}[I_{S_i,S_{c_i}}]$	${}^{S_1}\begin{bmatrix}21.75 & 0 & 0\\ 0 & 15.15 & 0\\ 0 & 0 & 36.6\end{bmatrix}$	$\mathrm{kg}\cdot\mathrm{m}^2$
Subpanel's center-of-mass location with respect to hinge point	${}^{S_i}\boldsymbol{r}_{S_{c_i}/S_i}$	${}^{S_i}[0, 1.8, 0]^T$	m
Position between hinge points	${}^{S_i}\boldsymbol{r}_{S_i/S_{i-1}}$	${}^{S_i}[0, 3.6, 0]^T$	m
Bending rotation axis	${}^{S_i}\hat{s}_i$	${}^{S_i}[1, 0, 0]^T$	— —
Torsional rotation axis	${}^{S_i}\hat{s}_i$	${}^{S_i}[0, 1, 0]^T$	— —
Bending linear spring constant	k_i	400	$(\mathrm{N}\cdot\mathrm{m})/\mathrm{rad}$
Bending linear damper constant	c_i	80	$(\mathrm{N}\cdot\mathrm{m})/\mathrm{rad}$
Torsional linear spring constant	k_i	20	$(\mathrm{N}\cdot\mathrm{m})/\mathrm{rad}$
Torsional linear damper constant	c_i	10	$(\mathrm{N}\cdot\mathrm{m})/\mathrm{rad}$

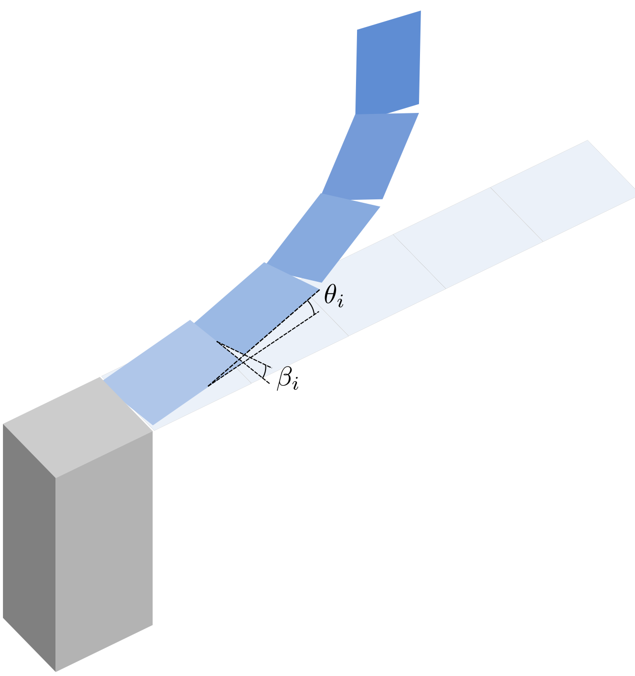

Fig. 11 Schematic of the spacecraft with a flexible panel. The lighter panel corresponds to the undeflected state. The bending angle is θ, and the torsional angle is β.

this model can capture complex dynamics beyond the rigid-body components typically considered in the first example scenario. Real-world applications would begin with a fully fledged CAD model of the solar array and the spacecraft, from which the properties of its primary modes would be extracted, such as modal frequencies and inertia fractions. Once collected, these properties would be converted into the spring and damper constants used in this example, which would be tuned to match the original flexing properties. For more details on how to model flexible dynamics using a lumped-mass approach, see Refs. [36,37].

The flexible panel scenario is fully documented in an open-source Basilisk example script.[§§§] The scenario documentation also contains an illustration video of the resulting flexing.[¶¶] A diagram of the spacecraft is shown in Fig. 11. The system starts at rest in rotation and then rotates to another inertial attitude. The goal is to excite the flexible panel as the spacecraft rotates from the initial to the final attitude. The simulation illustrates how flexing can be modeled using the finite-body approximation, which does not represent a realistic flexible panel.

The entire panel is 18 m long, 3 m wide, and 0.3 m thick. The flexible behavior is modeled by dividing the panel into rectangular plates or subpanels. The dimensions and mass of each subpanel depend on the number of subpanels used to discretize the full panel. Five subpanels are used for this simulation, and their properties are shown in Table 7. For simplicity, all subpanels have the same bending and torsional spring and damper coefficients. The coefficients are small, producing an exaggerated flexing motion that is noticeable in the spacecraft's attitude.

The time history for all bending and torsional angles is shown in Fig. 12. As expected, all angles start at 0, corresponding to the panel's undeflected state. As the spacecraft rotates from one attitude to another, the torque produced by the spacecraft's attitude-control devices imparts momentum to the panel, thereby exciting the flexible modes. Note that all bending or torsional angles deflect at the same frequency, resulting from choosing the same spring and damper constants for all bending or torsional axes.

The time history for the attitude error, expressed in modified Rodrigues parameters, and the angular velocity error is shown in Fig. 13. At the end of the simulation, the attitude and angular velocity errors converge to zero, indicating that the spacecraft exhibits robust attitude control despite a flexible appendage. Figure 13b shows the impact of the flexible appendage on the spacecraft's attitude, mostly along the $\boldsymbol{x}$ axis. While the other two axes exhibit the usual damped response, this axis shows a more complex response, particularly at the beginning of the simulation. This behavior is due to the panel being longer than it is wide, projecting along the $\boldsymbol{y}$ axis in a bending motion. Therefore, as the spacecraft rotates, that additional flexible inertia impacts the $\boldsymbol{x}$ axis more than the other axes.

VII. Conclusions

This paper presents a unified software architecture for developing and simulating sequentially rotating spacecraft components specific to the BSM. By deriving the equations of motion for any rotating component in a general way, it is possible to create a parent class that centralizes the physical description of this type of effector. Then, the user can use the module directly or inherit the parent class to create a specific component, such as a reaction wheel or a bending solar panel. This approach creates a library of specific components that need additional properties or different input/output connections tailored to the user's needs. Using the BSM implementation yields a software solution that is quick to set up and fast to execute. The capabilities of the general rotating appendage are demonstrated through two numerical examples, illustrating how this formulation can simulate controlled, articulated effectors or approximate the motion of flexing components.

[§§§]https://hanspeterschaub.info/basilisk/examples/scenarioFlexiblePanel.html.

[¶¶]https://youtu.be/kbcqUD4MW9c.

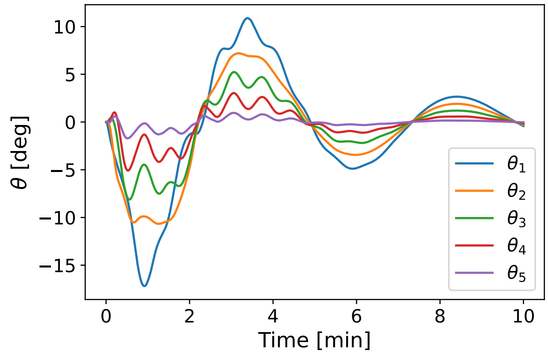

a) Bending angles

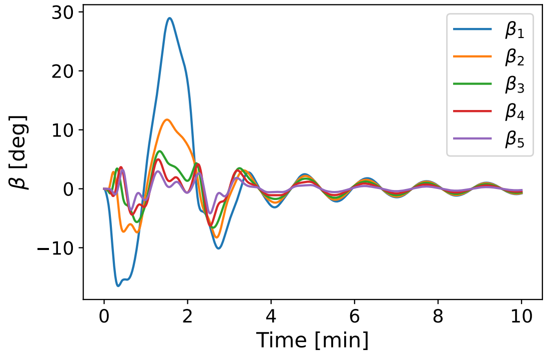

b) Torsional angles

Fig. 12 Time history of all degrees of freedom of the flexible panel.

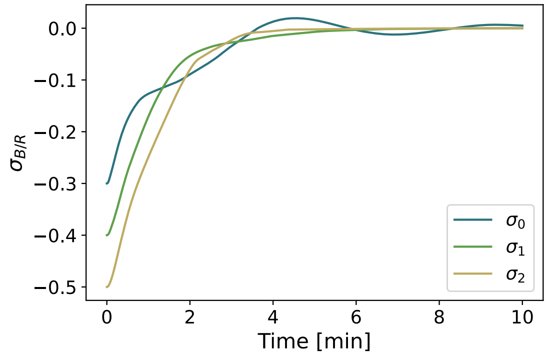

a) Attitude error

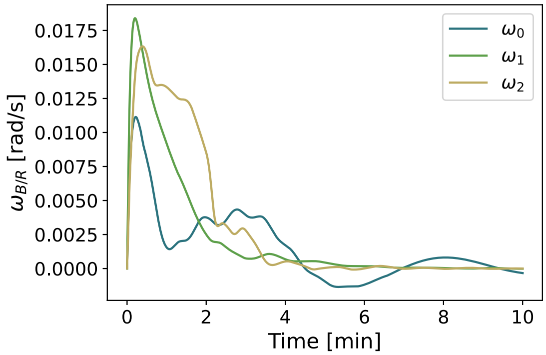

b) Angular velocity error

Fig. 13 Time history for the hub's states with a flexible panel.

Appendix A: Double-Summation Equalities

Double summations appear often in the development of the equations of motion, which can be represented generically as

$$\sum_{i=1}^{N}\sum_{j=1}^{i} f_{ij} \tag{A1}$$

While this form is valid, there are many instances in which it is preferable to reverse the i and j indices; that is, to place the second argument in the outer loop rather than the inner loop. This approach is particularly useful when state variables are explicitly written in the inner loop and must be put into the outer loop for the BSM. To show how the inner and outer loops can be flipped, Fig. A1 shows a diagram of a double summation.

Each dot represents a term in the double summation. On the left side, the iteration is performed rowwise by looping over j from 1 to i, so that all terms in each row are summed before proceeding to the next row. On the right, the iteration is done columnwise by looping j from i to N. These two approaches reorder the iteration order, swapping the inner and outer loops. From the diagram, it is trivial to find that the double-summation formula is

$$\sum_{i=1}^{N}\sum_{j=1}^{i} f_{ij} = \sum_{i=1}^{N}\sum_{j=i}^{N} f_{ji} \tag{A2}$$

Some double summations are truncated, with the outer loop starting at n instead of 1, which is represented by

$$\sum_{i=n}^{N}\sum_{j=1}^{i} f_{ij} \tag{A3}$$

Figure A2 shows a diagram of a truncated double summation to find the flipped summation formula. Again, on the left side, the iteration is performed rowwise by looping over i from n to N and over j from 1 to i. On the right side, the iteration is done columnwise. Because the summation is truncated, the iterations must be done in two parts: the first section is constant, where the inner loop goes from n to N, and the second section is decreasing, where the inner loop goes from i to N. Therefore, when flipping the inner and outer loops, two different double summations show up, which is shown in the following truncated double-summation formula:

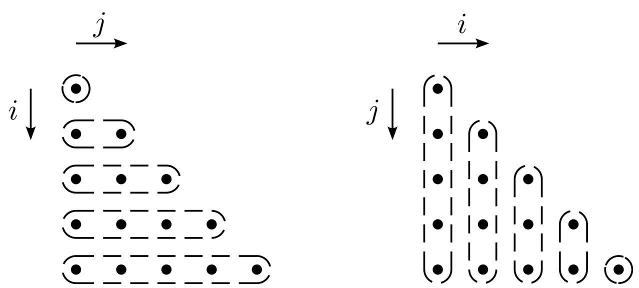

Fig. A1 Double-summation schematic.

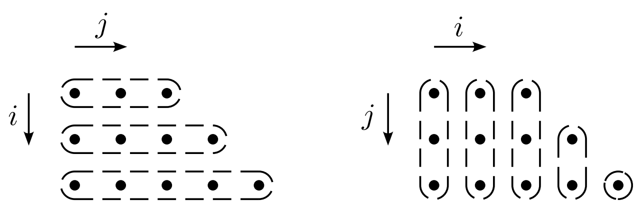

Fig. A2 Truncated double-summation schematic.

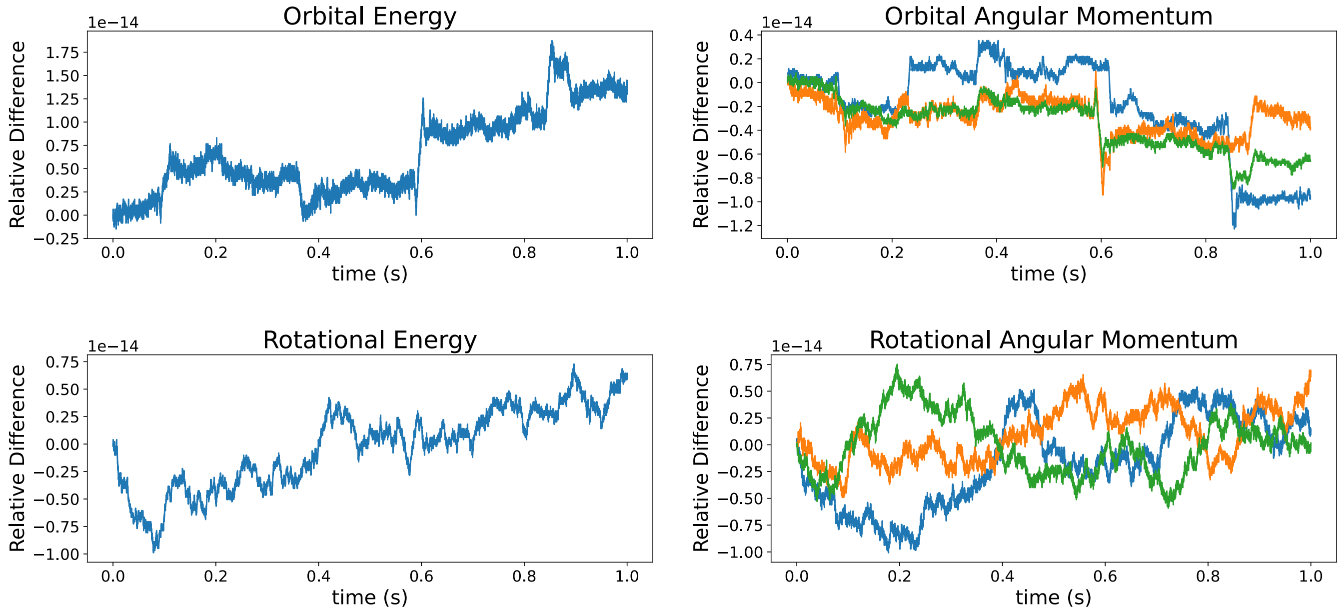

Fig. B1 Conservation plots for module verification.

$$\sum_{i=n}^{N}\sum_{j=1}^{i} f_{ij} = \sum_{i=1}^{n}\sum_{j=n}^{N} f_{ji} + \sum_{i=n+1}^{N}\sum_{j=i}^{N} f_{ji} \tag{A4}$$

Appendix B: Dynamic Equations of Motion Verification Procedure

A fundamental step in any simulation concerns the verification of the equations developed. Because the equations of motion represent a physical, mechanical system, conservation laws can be used to verify that both the software implementation and the underlying equations are correct. This verification is impossible if some cross-coupling terms, even the smaller ones, are removed. In particular, the principles of energy and angular-momentum conservation can be used to verify that the model satisfies physical laws. In an environment where only conservative forces and torques are present, the energy and angular momentum of the entire system must be conserved. In other words, the energy (a scalar) and the angular momentum, expressed in the inertial frame $\mathcal{N}$ (a vector), must not change throughout the simulation.

Furthermore, energy and angular momentum can be separated into their orbital and rotational components, which must be conserved. This separation arises from the large magnitude difference between the orbital and rotational parts. Failing to separate the two contributions could lead to minor errors in one rotational component going undetected, as the orbital term overwhelms the result.

In line with the BSM, the energy and angular momentum equations are written to separate the hub and center-of-mass properties from the specific effector contributions. Only the effector contributions to the rotational terms are shown; see Ref. [18] for details on the full equations. The contribution to the rotational energy is

$$T_{\text{rot}} = \sum_{i=1}^{N}\left(\frac{1}{2}\boldsymbol{\omega}_{\mathcal{S}_i/\mathcal{N}}\cdot[I_{\text{S}_i,S_{c_i}}]\boldsymbol{\omega}_{\mathcal{S}_i/\mathcal{N}} + \frac{1}{2}m_{\text{S}_i}\dot{\boldsymbol{r}}_{S_{c_i}/B}\cdot\dot{\boldsymbol{r}}_{S_{c_i}/B}\right) \tag{B1}$$

while the contribution to the rotational angular momentum is

$$\boldsymbol{H}_{\text{rot},C} = \sum_{i=1}^{N}([I_{\text{S}_i,S_{c_i}}]\boldsymbol{\omega}_{\mathcal{S}_i/\mathcal{N}} + m_{\text{S}_i}\boldsymbol{r}_{S_{c_i}/B}\times\dot{\boldsymbol{r}}_{S_{c_i}/B}) \tag{B2}$$

The conservation laws are verified by a simulation that includes the effectors modeled in this paper, and the results are shown in Fig. B1. The energy and angular momentum at each time step are compared with their values at $t = 0$. This comparison is performed by dividing the difference between the two values by the initial value, yielding a relative difference. Due to the finite number of bits in computers, the relative difference is never zero but rather very close to machine precision, on the order of 10^{-15}. Moreover, the relative difference does not stay completely constant. Instead, it appears to be a random walk, which is common with fixed-time-step integrators.

Acknowledgment

The La Caixa Foundation (ID 100010434) supported this work through the Postgraduate Fellowships Abroad program under agreement LCF/BQ/EU22/11930093.

References

[1] "NASA—NSSDCA—Spacecraft—Details—nssdc.gsfc.nasa.gov," 2022, https://nssdc.gsfc.nasa.gov/nmc/spacecraft/display.action?id=1957-001B [retrieved 21 July 2023].

[2] DeLucas, L. J., "International Space Station," *Acta Astronautica*, Vol. 38, Nos. 4–8, 1996, pp. 613–619. https://doi.org/10.1016/0094-5765(96)00056-2

[3] Aikenhead, B. A., Daniell, R. G., and Davis, F. M., "Canadarm and the Space Shuttle," *Journal of Vacuum Science & Technology A: Vacuum, Surfaces, and Films*, Vol. 1, No. 2, 1983, pp. 126–132. https://doi.org/10.1116/1.572085

[4] Sachdev, S., "Canadarm—A Review of Its Flights," *Journal of Vacuum Science & Technology A: Vacuum, Surfaces, and Films*, Vol. 4, No. 3, 1986, pp. 268–272. https://doi.org/10.1116/1.573952

[5] Hiltz, M., Rice, C., Boyle, K., and Allison, R., "Canadarm: 20 Years of Mission Success Through Adaptation," *International Symposium on Artificial Intelligence, Robotics and Automation*, 2001, pp. 1–8.

[6] Redd, N. T., "Bringing Satellites Back from the Dead: Mission Extension Vehicles Give Defunct Spacecraft a New Lease on Life," *IEEE Spectrum*, Vol. 57, No. 8, 2020, pp. 6–7. https://doi.org/10.1109/MSPEC.2020.9150540

[7] Howlett, J., Forshaw, J., and Valhondo, V., "UK ADR: The UK Space Agency's Active Debris Removal Mission," *2nd International Orbital Debris Conference*, Vol. 2852, 2023, p. 6075.

[8] Biesbroek, R., Aziz, S., Wolahan, A., Cipolla, S.-f., Richard-Noca, M., and Piguet, L., "The Clearspace-1 Mission: ESA and Clearspace Team up to Remove Debris," *8th European Conference on Space Debris*, April 2021, pp. 1–3.

[9] Kiner, L., Schaub, H., and Allard, C., "Spacecraft Backsubstitution Dynamics with General Multibody Prescribed Subcomponents," *Journal of Aerospace Information Systems*, Vol. 22, No. 8, 2025, pp. 703–715. https://doi.org/10.2514/1.I011491

[10] Markley, F. L., and Crassidis, J. L., *Fundamentals of Spacecraft Attitude Determination and Control*, 1st ed., Springer, Berlin, 2014. https://doi.org/10.1007/978-1-4939-0802-8

[11] Liu, L., *Jitter and Basic Requirements of the Reaction Wheel Assembly in the Attitude Control System*, Maschusetts Inst. of Technology, Cambridge, MA, 2007.

[12] Gutierrez, H. L., "Performance Assessment and Enhancement of Precision Controlled Structures During Conceptual Design," Ph.D. Thesis, Massachusetts Inst. of Technology, Cambridge, MA, 1999.

[13] Kiner, L., Allard, C., and Schaub, H., "Two-Axis Gimbal Simulation Overview for the Emirates Mission to the Asteroid Belt," *AAS Guidance, Navigation and Control Conference*, AAS Paper 25-013, Springfield, VA, 2025.

[14] Kiner, L., Allard, C., and Schaub, H., "Prescribed Motion Dynamics for Spacecraft Solar Array Deployment," *AAS Guidance and Control Conference*, AAS Paper 24-123, Springfield, VA, Feb. 2024.

[15] Vaz Carneiro, J., Allard, C., and Schaub, H., "General Dynamics for Single and Dual-Axis Rotating Rigid Spacecraft Components," *AIAA Journal of Spacecraft and Rockets*, Vol. 61, No. 4, 2024, pp. 1099–1113.
https://doi.org/10.2514/1.A35865

[16] Alcorn, J., Allard, C., and Schaub, H., "Fully Coupled Reaction Wheel Static and Dynamic Imbalance for Spacecraft Jitter Modeling," *AIAA Journal of Guidance, Control, and Dynamics*, Vol. 41, No. 6, 2018, pp. 1380–1388.
https://doi.org/10.2514/1.G003277

[17] Allard, C., Schaub, H., and Piggott, S., "General Hinged Solar Panel Dynamics Approximating First-Order Spacecraft Flexing," *AIAA Journal of Spacecraft and Rockets*, Vol. 55, No. 5, 2018, pp. 1290–1298. https://doi.org/10.2514/1.A34125

[18] Allard, C., Diaz-Ramos, M., Kenneally, P. W., Schaub, H., and Piggott, S., "Modular Software Architecture for Fully-Coupled Spacecraft Simulations," *Journal of Aerospace Information Systems*, Vol. 15, No. 12, 2018, pp. 670–683.
https://doi.org/10.2514/1.I010653

[19] Allard, C., Diaz-Ramos, M., and Schaub, H., "Computational Performance of Complex Spacecraft Simulations Using Back-Substitution," *Journal of Aerospace Information Systems*, Vol. 16, No. 10, 2019, pp. 427–436.
https://doi.org/10.2514/1.I010713

[20] Vaz Carneiro, J., and Schaub, H., "Spacecraft Dynamics with the Backsubstitution Method: Survey and Capabilities," *AAS Spaceflight Mechanics Meeting*, AAS Paper 25-232, Springfield, VA, 2025.

[21] Rodriguez, G., Jain, A., and Kreutz-Delgado, K., "A Spatial Operator Algebra for Manipulator Modeling and Control," *International Journal of Robotics Research*, Vol. 10, No. 4, 1991, pp. 371–381.
https://doi.org/10.1177/027836499101000406

[22] Jain, A., and Rodriguez, G., "Recursive Flexible Multibody Dynamics Using Spatial Operators," *Advances in Factories of the Future, CIM and Robotics, Manufacturing Research and Technology*, edited by M. Cotsaftis, and F. Vernadat, Vol. 16, Elsevier, Amsterdam, The Netherlands, 1993, pp. 345–358, https://www.sciencedirect.com/science/article/pii/B9780444898562500363.
https://doi.org/10.1016/B978-0-444-89856-2.50036-3

[23] Rodriguez, G., Jain, A., and Kreutz, K., "Spatial Operator Algebra Framework for Multibody System Dynamics," *Proceedings of the 3rd Annual Conference on Aerospace Computational Control*, Vol. 1, 1989.

[24] Alcorn, J., Allard, C., and Schaub, H., "Fully-Coupled Dynamical Jitter Modeling of Variable-Speed Control Moment Gyroscopes," *AAS/AIAA Astrodynamics Specialist Conference*, AAS, Springfield, VA, 2017, pp. 1–11.

[25] Jain, A., "Darts-Multibody Modeling, Simulation and Analysis Software," *Multibody Dynamics 2019: Proceedings of the 9th ECCOMAS Thematic Conference on Multibody Dynamics*, Springer, Berlin, 2020, pp. 433–441.

[26] Martin, R. C., *Clean Code: A Handbook of Agile Software Craftsmanship*, Pearson Education, London, 2009.

[27] Martin, R. C., *Clean Architecture*, Prentice Hall, Upper Saddle River, NJ, 2017.

[28] Kane, T. R., and Levinson, D. A., *Dynamics, Theory and Applications*, McGraw Hill, New York, 1985.

[29] Roithmayr, C. M., and Hodges, D. H., "Dynamics: Theory and Application of Kane's Method," 2016.

[30] Schaub, H., and Junkins, J. L., *Analytical Mechanics of Space Systems*, 4th ed., AIAA Education Series, AIAA, Reston, VA, 2018.
https://doi.org/10.2514/4.105210

[31] Géradin, M., and Rixen, D. J., *Mechanical Vibrations: Theory and Application to Structural Dynamics*, Wiley, Hoboken, NJ, 2014.

[32] Panicucci, P., Allard, C., and Schaub, H., "Spacecraft Dynamics Employing a General Multi-Tank and Multi-Thruster Mass Depletion Formulation," *Journal of Astronautical Sciences*, Vol. 65, No. 4, 2018, pp. 423–447.
https://doi.org/10.1007/s40295-018-0133-0

[33] Allard, C., Maxwell, J., and Schaub, H., "A Transport Theorem for the Inertia Tensor for Simplified Spacecraft Dynamics Development," *International Astronautical Congress*, Paris, France, 2022, pp. 1–6.

[34] Allard, C. J., "Modular Software Architecture for Complex Multi-Body Fully-Coupled Spacecraft Dynamics," Ph.D. Thesis, Univ. of Colorado Boulder, 2018.

[35] Kenneally, P. W., Piggott, S., and Schaub, H., "Basilisk: A Flexible, Scalable and Modular Astrodynamics Simulation Framework," *Journal of Aerospace Information Systems*, Vol. 17, No. 9, 2020, pp. 496–507.
https://doi.org/10.2514/1.I010762

[36] Shabana, A. A., *Dynamics of Multibody Systems*, Cambridge Univ. Press, Cambridge, England, U.K., 2020.

[37] Haug, E. J., *Computer Aided Kinematics and Dynamics of Mechanical Systems*, Vol. 1, Allyn and Bacon Boston, MA, 1989.

D. Casbeer
Associate Editor